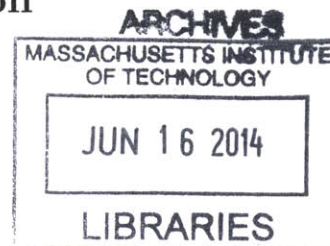# Multi-parameter Control for Centrifugal Compressor Performance Optimization

by

Sebastien Mannai

S.M., Ecole Centrale Paris (2013)
S.M., University of Paris XI Saclay (2013)

Submitted to the Department of Aeronautics and Astronautics
in partial fulfillment of the requirements for the degree of

Master of Science in Aeronautics and Astronautics

at the

MASSACHUSETTS INSTITUTE OF TECHNOLOGY

June 2014

Author . . . **Signature redacted**
....
Department of Aeronautics and Astronautics
May 22, 2014

Certified by **Signature redacted**
....
Choon Sooi Tan
Senior Research Engineer
Thesis Supervisor

Accepted by . . . **Signature redacted**
....
Prof. Paulo C. Lozano
Associate Professor of Aeronautics and Astronautics
Chair, Graduate Program Committee

Multi-parameter Control for Centrifugal Compressor Performance Optimization

by

Sebastien Mannai

Abstract

The potential performance benefit of actuating inlet guide vane (IGV) angle, variable diffuser vane (VDV) angle and impeller speed to implement a multi-parameter control on a centrifugal compressor system is assessed. The assessment consists of first developing a one-dimensional meanline model for estimating performance of centrifugal compressor system followed by the formulation of a control framework incorporating the meanline model. Performance estimate of a representative centrifugal compressor system with adjustable IGV angle, VDV angle and impeller speed using the meanline model is in accord with available test data. The impeller performance estimate based on the meanline model is also in accord with computed results from Reynolds Average Navier-Stokes Equations. The simple control framework can be used to optimize on the fly the compressor operation to meet a specific mission requirement by selecting an appropriate combination of impeller speed, IGV and VDV angle settings. Desirable flow configurations with the required performance in response to specified operating needs have been obtained to serve as illustrations on the practical utility of the control framework. Results provide guidelines and attributes of compressor for achieving the required performance and operation at the system level through prioritizing the actuation of the adjustable parameters; for instance impeller speed would provide a high level of leverage to affect the compressor performance on an effective basis and that the IGV angle should be confined to a specified range. While the results have not been assessed in an experimental setting, they are used to design and plan an experimental program for evaluating the proposed simple multi-parameter control strategy. Flexibility have been incorporated into the formulation to allow the refinement and updating of the model for improved accuracy and fidelity.

3

Acknowledgments

Contents

List of Figures

10

List of Tables

Chapter 1

Introduction

1.1 Motivation

Centrifugal compressor systems deployed in the industry are required to operate twenty four hours a day seven days a week with minimum down time. This is especially true for the wastewater aeration market. Compressors are used to supply large quantities of air at the bottom of water reservoir, creating small air bubbles to oxygenate the water, allowing bacteria growth. The compressors commonly used for wastewater management have a relatively low pressure ratio, usually less than 2. This pressure rise is achievable by a single stage machine. A huge amount of clean air has to be provided while minimizing the carbon footprint and this aeration process consumes about 50% of the energy usage of the whole plant; this explains why any improvement in the compressor system efficiency has a large impact on a water treatment infrastructure energy usage. As such their operation at high thermodynamic efficiency across a wide operating range is of paramount importance to the customers.

Extending the compressor performance and operable range to meet the needs of a specific engineering mission is an important aspect of centrifugal compressor engineering. Strategies to quantitatively assess the potential for extending compressor operating range while maintaining operation at high efficiency must be developed. This can be done by determining the drivers that set the requirements for the broadest

operable range with high efficiency retention.

1.2 Technical Background

1.2.1 Compressor System Design
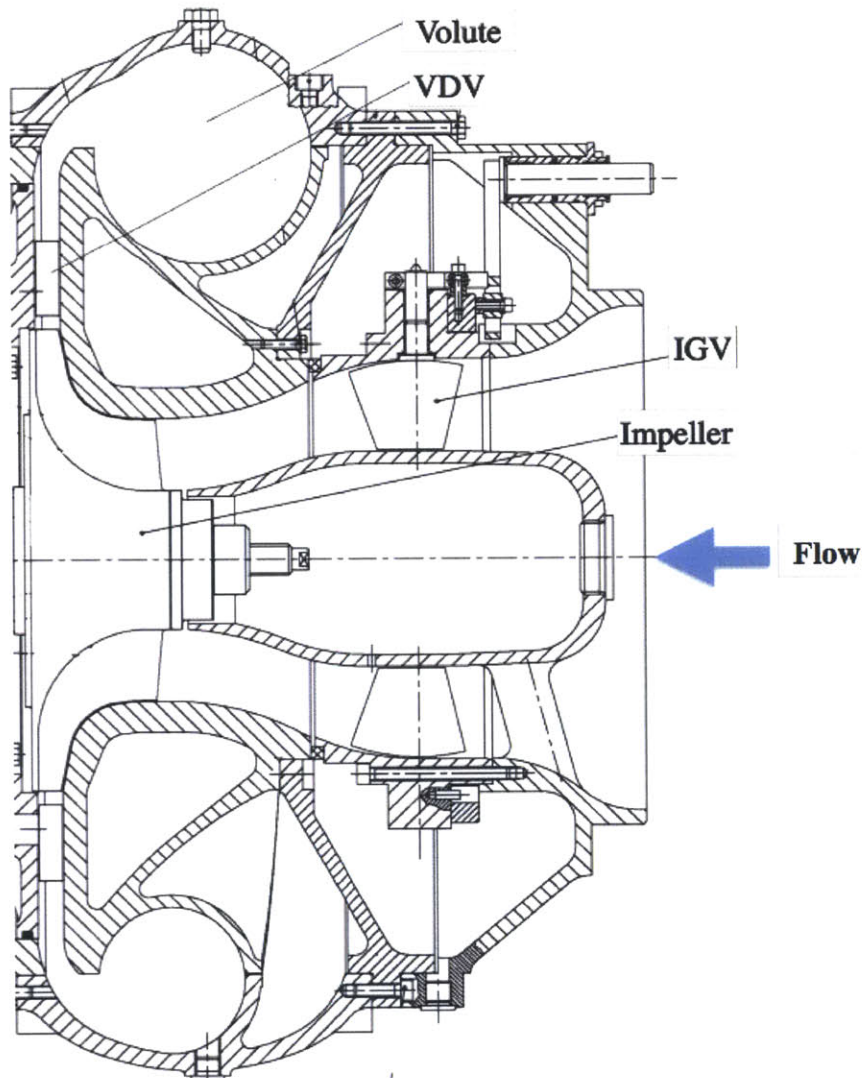
Figure 1-1: Section of a centrifugal compressor with adjustable guide vanes (IGV) and adjustable diffuser vanes (VDV)

A centrifugal compressor increases the fluid pressure by adding kinetic energy to the flow with a rotating impeller. This excess kinetic energy is converted into a pres-

sure rise in the diffuser and to a lesser extent in the volute. A representative flow path is shown in Figure 1-1. Since the flow leaves the impeller with a high velocity the diffuser has to be matched to flow else the losses will be significant.

The design studied here uses a diffuser with several vanes. Vaned diffuser are known to achieve higher efficiency than their vaneless counterpart, but they have a limited range of efficient operation as the vanes angle are designed for a specific operating point; one solution to alleviate this issue is to use adjustable vanes. However the machine cost and complexity increases and new losses (such as tip-gap flow losses) are also created so the benefits of Variable Diffuser Vanes (VDV) has to be evaluated. Before the impeller there can be a row of Variable Inlet Guide Vanes (IGV) that are used to add a precise amount of swirl to the flow, reducing the impeller pressure rise and allowing the compressor to be used at lower mass flow. Again adding this component increases the machine cost and creates new losses that have to be evaluated.

1.2.2 Compressor System Characteristics

A compressor is evaluated based on several characteristic metrics:

- its pressure ratio

- the lowest and highest mass flow that can be pumped

- the efficiency (or power consumption) at each mass flow rate

- the cost of the system

The pressure ratio is fixed by the customer requirement and is often required to have a fixed value throughout the usable range. However all the other characteristics are strongly inter-dependent and a trade-off study has to be implemented. The range of usable mass flow can be increased with adjustable Inlet Guide Vanes but the machine cost will increases and the efficiency will drop.

Usually a cheaper machines that is easier to manufacture is less efficient than one

that has a complex 3D impeller that has to be machined with computer controlled equipment instead of being casted.

1.3 Objectives

1.3.1 Research Objectives

The goal of this research is to, first, identify what are the parameters of high leverage that affect centrifugal compressor performance, followed by establishing potential means of achieving near matching of centrifugal compressor components at all desirable operating points. Some of the key parameters that are thought to have a high leverage on compressor performance characteristics are the compressor speed, the guide vane angle setting and the diffuser vane angle setting; however there could be others that are to be identified during the course of the research. In light of this, formulating an effective control strategy (passive, active or a combination of both) designed for a specific mission that achieves desirable compressor performance requirements at an optimal cost is another goal for this research.

This thesis is aimed at enhancing centrifugal compressor efficiency and operability by seeking quantitative answer to the following research questions:

- What are the attributes of centrifugal compressor design and operation for achieving a broad operable performance characteristic with high efficiency retention?

- What are the parameters of high leverage that affect centrifugal compressor performance on an effective basis to meet its mission requirements?

- What is an effective control strategy for achieving desirable compressor performance requirements for a specified mission at an optimal cost?

- What should the functional dependence of the non-dimensional performance parameters be to improve the controllability and behaviour of the compressor on a beneficial basis?

16

A design-implement analyses and a reduced order modelling will be developed in order to:

- Assess drivers that set loss and flow blockage generation in critical flow paths

- Determine whys and hows of performance enhancement for broadest operable range with high efficiency retention

- Determine influences, limitations, and possible mitigation/control strategy for near matching of compressor components at all required operating points

- Define physical experiments for assessments of ideas and results

- Establish design guidelines for optimum performance enhancement

1.3.2 Engineering Requirements for Specific Mission

Typically a customer for centrifugal compressor system used in water management infrastructure defines a certain number of test points (usually 4) and specifies for each test point a temperature, humidity, inlet pressure (atmospheric pressure generally), an outlet pressure, the mass/volume flow, the power, and an evaluated factor of importance. This last factor indicates how important is a test point for a customer, a low number indicates the compressor will not be used often at those conditions. An example of a customer requirement is illustrated in table 4.2.

Table 1.1: Example of four specified Performance test Points

Inlet Pressure	Outlet Pressure	Flow	Power HP	Evaluated Factor
14.35 psia	20.61 psia	4164 acfm	130.7	5%
14.35 psia	20.61 psia	3331 acfm	105.0	40%
14.35 psia	20.61 psia	2498 acfm	80.9	45%
14.35 psia	20.61 psia	1874 acfm	64.3	10%

It is of importance to note that if the power consumed is larger than the specified one, a large penalty must be paid to the customer. The concept of optimizing

a compressor within the specified constraints is to minimize the power used at each test point while still taking into account the relative importance of each test point.

An industrial compressor specific for the waste water treatment market was studied. The experimental data that was initially provided has been normalized using the stage loading coefficient and the flow coefficient defined bellow.

- The stage loading/pressure rise coefficient:$\psi = \frac{\Delta h}{U_2^2}$

- The flow coefficient:$\phi = \frac{V_{n2}}{U_2}$

- The normalized flow coefficient:$\Phi = \frac{\phi}{\phi_{max}}$

Data has been gathered for various RPM and various vanes angles as illustrated in Figure 1-2 where the VDV is fixed and the IGV is a variable. Several compressors map similar to Figure 1-2 were available, for various IGV and VDV positions and were used as benchmark to assess the mean-line model.
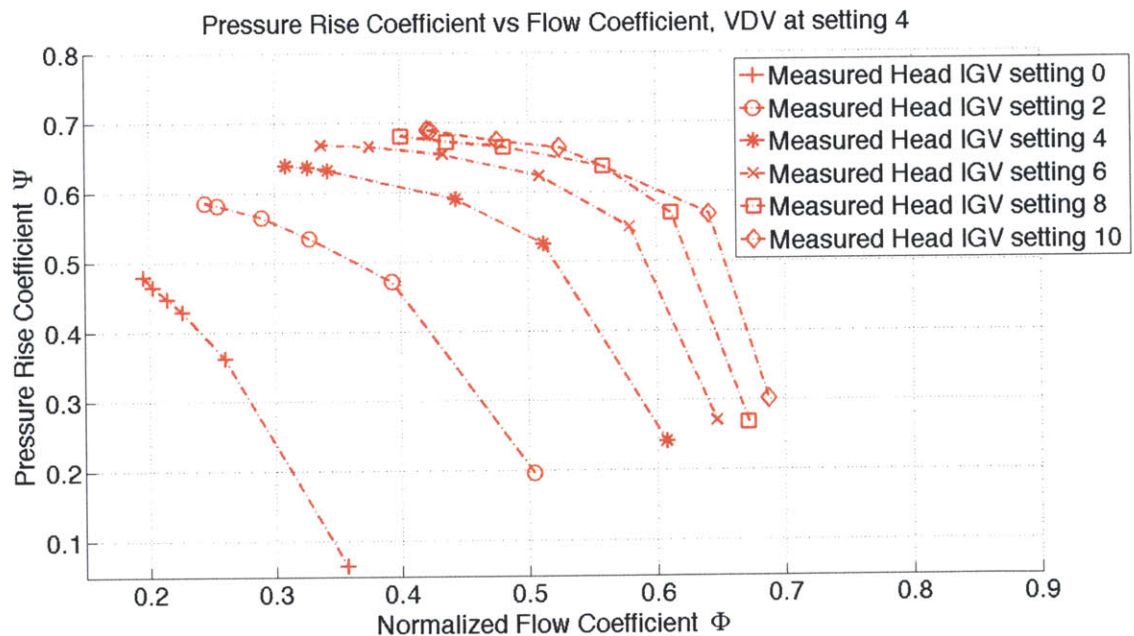
Figure 1-2: Compressor map for the VDV fixed and different IGV angles, no swirl is added to the flow at an IGV setting of 10

1.4 Research Contributions

The contributions of this thesis are delineated below:

- Formulation and development of physically consistent loss models for centrifugal compressors with variable inlet guide vanes and diffuser vanes. A meanline model for estimating centrifugal compressor performance incorporating the loss models yields results in accord with test data and computed solution from the Reynolds Averaged Navier Stokes equations.

- Adjustable IGV used at angle setting above threshold value result in substancial efficiency drop (large IGV angles are to be used only if it is critical to reach low flow coefficient with no concerns on the compressor efficiency penalty).

- The VDV has a significant impact on the operable range and there is a trade-off between efficiency and broad operating range; this is confirmed by the experimental data. The added complexity of adjustable diffuser vanes is justified only if the range of required mass flow is large enough.

- The impeller tip-speed, which is adjusted by changing the drive motor RPM, is the most effective way to adjust the impeller head.

- Formulation and implementation of an effective yet simple control framework that can accommodate compressor configuration that have adjustable inlet and diffuser vanes or ones that have only adjustable inlet vanes. It provides enabling strategy to:

  1. Maximize the efficiency and use the full potential of the system at any working point.

  2. Reliably go from one working point to another

1.5 Organisation of Thesis

This thesis is organized as follows:

Chapter 2

Chapter Two presents the technical approach used throughout this research and the methodology used to compare the analytical work and the experimental one.

Chapter 3

Chapter Three provides a detailed analysis of the meanline model and the associated loss mechanisms for each of the components in the centrifugal compressor system.

Chapter 4

Chapter Four provides a description of the control framework that drives the whole system and how it uses the mean-line model to optimize and match system to operating needs.

Chapter 5

Chapter Five describes the use of CFD to evaluate losses occurring in the impeller. The results are also used to assess the meanline model key assumptions.

Chapter 6

Chapter Six describes the experimental protocol that allows one to extract key parameter to estimate the losses in the machine as well as the implementation of the proposed control framework on a compressor test rig.

Chapter 7

Chapter Seven presents a summary of the findings as well as recommendation for future work that builds upon the present work.

Chapter 2

Technical Approach

2.1 Introduction

Meanline model of a centrifugal compressor can provide an estimate of the key performance metrics of the machine. A meanline model is flexible and allows one to estimate the performances of centrifugal compressor effectively in contrast to performance estimation based on CFD or experimental measurements. The model should not only be of "reasonable accuracy" (this will be more accurately defined in the following chapters), but more importantly the qualitative parametric trends should be consistent on a physical basis. This allows the designer to choose the right parameters to optimize a system and enhance its turndown performance and/or its efficiency. This greatly reduces the number of iterations based on CFD necessary to design the system and to determine the range of variations of parameters in a specific engineering mission.

2.2 Framework & Previous Work

2.2.1 Assumptions

The loss models are used to provide an estimate of a system efficiency. The goal is to have an adequate model for a representative centrifugal compressor of low pressure ratio in subsonic flow. There has been previous work on formulating loss models for

estimating axial compressor performance. In particular David K. Hall's work on "Performance Limits of Axial Turbomachine Stages" has been useful for formulating the loss models in centrifugal compressors [7], [6]. The model developed by Dickens & Day [4] to relate axial compressor stage efficiency and blade loading using boundary layer calculations was adapted for use used on centrifugal machines. The model developed here is a one-dimensional, meanline and quasi-steady model. It approximates the impeller blade surface velocity distribution as rectangular. It also assumes no separation occurs in the centrifugal compressor flow path.

2.2.2 Formulation of Mean Line Model

Several authors have studied loss mechanism in depth. Denton [1] provides a detailled analysis of loss mechanisms in turbomachines while Cumpsty describes losses specific to Centrifugal Compressors [5] . Denton's analysis on loss generation was especially useful when evaluating the viscous losses generated on wetted surface. His model for estimating tip-gap loss was adapted for evaluating the losses due to flow through the impeller blade gap and the variable diffuser vane gap.

Hall [7] has formulated and developed loss models for estimation of an upper limit of the stage efficiency in axial compressors, but as far as the author knows there has been no such work on Centrifugal machines, let alone the incorporation of such model based on physical loss mechanisms within a control framework to improve the overall system operation on an optimal basis.

Various metrics are used for characterizing the performance of the system set by its components. They are presented in a top-down manner as follows.

On the system basis, the only two relevant parameters are the mechanical efficiency and the turndown of the machine. The first is directly linked to the electrical power consumption of the machine and is defined by the power transmitted to the flow over the electrical power used; it takes into account not only the machine isentropic efficiency but also the efficiency of the motor and the gears driving it.

$$\eta_{system} = \frac{P_{flow}}{P_{electric}} \tag{2.1}$$

The second metric indicates if the compressor can be used for a broad range of flow coefficient (or mass flow). It is defined as

$$Turndown = \frac{\dot{m}_{min}}{\dot{m}_{max}} = \frac{\phi_{min}}{\phi_{max}} \tag{2.2}$$

If we limit ourselves to the fluid part of the compressor (i.e. we ignore what is driving the impeller and the losses that are generated by external sub-systems), the compressor isentropic efficiency can be calculated by evaluating the product of all the components efficiency:

$$\eta_{compressor} = \frac{P_{flow}}{P_{impeller}} = \prod_{j=components} \eta_j \tag{2.3}$$

On a component level of the machine, it is necessary to determine and quantify the sources of various losses. Therefore the isentropic efficiency is used. It is defined by the normalized sum of all the sources i of loss Φ_i of each component, with $\Phi_i = T_i \Delta S_i$. Those sources of losses i can be created by various phenomena such as mixing of flow from a tip-gap with the main flow and are described in the following chapter.

$$\eta_{component} = 1 - \frac{\sum_i \Phi_i}{\dot{m}\Delta h_t} \tag{2.4}$$

The decrement in isentropic efficiency associated with loss generation in a component can be converted into a stagnation pressure loss for direct comparison to the measured data. This isentropic efficiency is closely linked to the total pressure drop and both quantities can be used interchangeably. V_{n2} is the impeller meridional velocity at the exit station, T_t is the flow stagnation temperature.

$$P_{t_{out}} = P_{t_{in}}.exp(-(1 - \eta_{isentropic})\frac{\phi^2.V_{n2}^2}{\psi}.R_{air}.T_t) \tag{2.5}$$

The total pressure being more useful as it is directly the measured quantity in

tests or experiments.

On a sub-component level, the entropy generation is analysed to determine the source of inefficiencies from a specific source of loss. Φ_j is the dissipation created by a specific source of loss with the loss created in a component $\Phi_i = \sum_j \Phi_j$, with Φ_i the loss of the component i and Φ_j the sources of loss inside component i.

2.2.3   Development of a Control Strategy
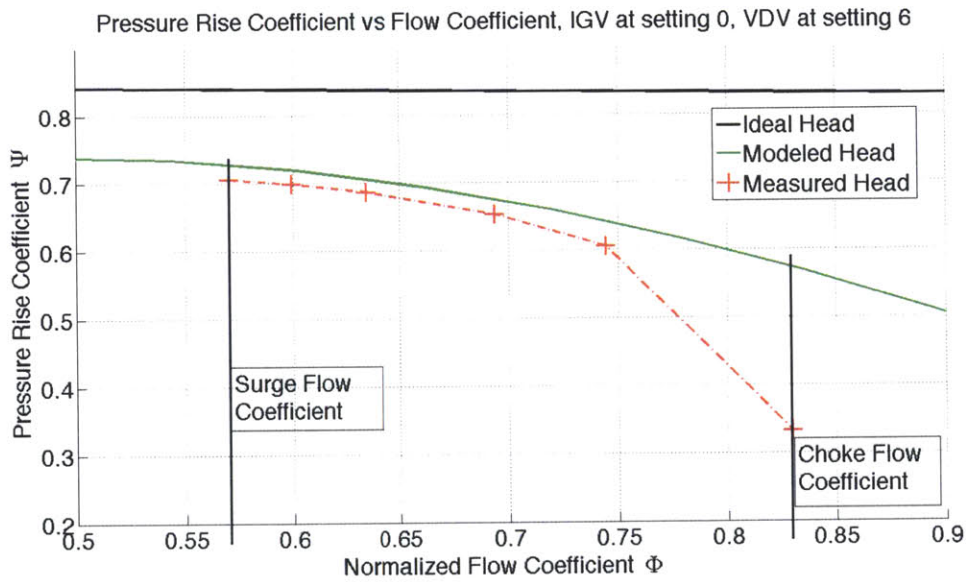
Figure 2-1: Computed and measured compressor map with choke point and surge point

A control strategy has been formulated based on the results provided by the 1D meanline model. It uses the model to evaluate different efficiencies at different flow conditions and optimize the system by choosing the adjustable parameters (IGV,VDV,RPM) to yield the most efficient operation. It is also used to provide a mean to plan out a sequence of steps to achieve a quasi-steady transient change of flow conditions (i.e. when going from one working point to the other) acceptable on an operational basis. To do so the surge criteria described by Cumpsty was adopted. The surge boundary needs to be evaluated and a safety margin is then applied to enable the compressor to operate within its operable range. The surge point corresponds to

24

the measured operating point with the smallest achievable flow coefficient for which the compressor is in stable operation. In Figure 2-1, the measured surge point is indicated. The measured, computed (based on the meanline model formulated in this thesis), and ideal characteristics are also shown.

2.2.4   Assessment of the Meanline Model with CFD

As explained above, a typical compressor map does not give any information concerning the distribution of losses between the different components of the machine, nor does it give information about the relative importance of different losses for each component. To judge the validity of the 1D model, it was decided to assess it by comparing it to both CFD RANS simulations and to experimental data measurements. The CFD is used to model the impeller and it is used to assess the different assumptions made with the 1D model as well as estimating the losses from the impeller and the inlet guide vanes. Measurements within the vaneless space allow to experimentally assess the adequacy of both the CFD model and the 1D model for the impeller and the IGV. The combined efficiency of diffuser and volute can be deduced from both the CFD and the experimental measurements.

2.2.5   Assessment of the Ideas and the Control Strategy on Compressor Rig

There has been a great deal of studies on experimental data measurements and probes, the work of R.C Pankhurst [10] was useful by providing guidelines for designing the probes. Several studies measure the static pressure within a Centrifugal machine either on the hub or the shroud [15], but no publication were found on measuring total pressure and flow angle by modifying adjustable diffuser vanes. Those previous studies were used to design a diffuser vane that incorporate a flow angle probe and a total pressure measurement probe. The experimental protocol for the acquisition of data and execution of the control framework on a compressor rig has been established and proposed but has yet to be implemented.

2.3   Limits of a 1D model
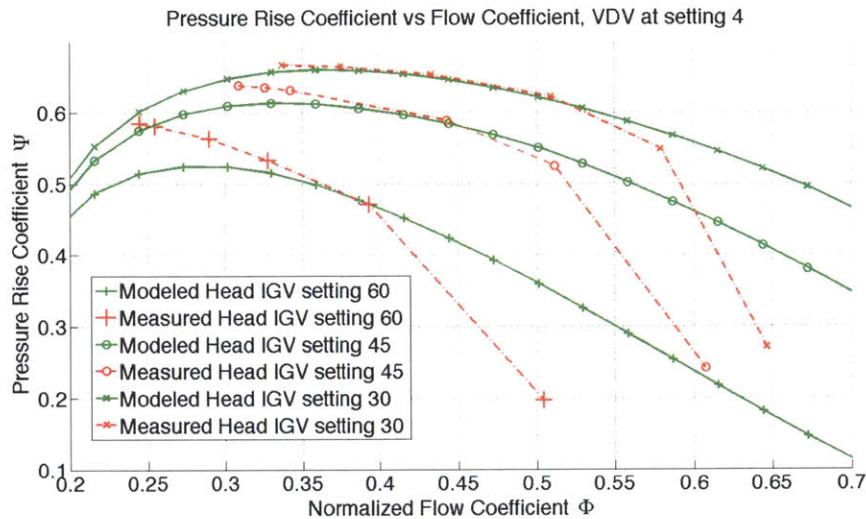
Figure 2-2: Computed compressor map for increasing IGV angle with VDV set at setting 4

The 1D model provides useful result, and the many evaluated quantities are within the margin of error of the experimental compressor map. However there is no way to know if the loss distribution between each component is valid, only the total sum of the losses can be compared to a measured compressor map. Without assessing the model with CFD and/or advance experimental data it is not possible to know what is the effect of modifying a parameter on a component level.

Furthermore, the model shows its limits when it is used close to the surge point or close to the choke point. However these operating conditions are normally to be avoided respectively because there is a risk of damaging the equipment or because the machine is inefficient at those working points. Close to surge the flow separates from the impeller and there are large recirculation areas and the losses induced are beyond the scope of the model. The impeller blade surface rectangular velocity distribution assumed is no longer a good approximation. This can be seen on Figure 2-2 where the model is accurate for low IGV settings but as the IGV angle is increased the difference between the measured and the computed head diverges. This difference is maximum at the surge and choke point. The model is also limited when large vanes

angles are used, as regions of large flow separation are to be expected.

2.4 Summary

This chapter presents the technical approach that consists of formulating a mean line model for the components of a centrifugal compressor system and establishing a control framework based on that model to drive the compressor to maintain optimal performance. The attributes of the model and its control framework are to be assessed using both CFD and experimental measurements. The control framework will also be assessed experimentally on the compressor rig. At a sub-component scale the entropy generation is evaluated and analysed but the isentropic efficiency will be the key metric used to compare different design. The overall efficiency of the full system will be used when formulating the control framework.

Chapter 3

A Mean-Line Model for estimating Centrifugal Compressor System Performance

3.1 Introduction

In this chapter we first analyse what are the sources of loss that will be incorporated into the model. Some loss mechanism are only relevant to specific area of the flow so each component and section of the compressor is analysed to determine what loss should be taken into account for that component. The surge point is estimated based on a criteria described in Cumpsty [5]. Using the different loss models the compressor map can be computed and assessed against available data as seen on Figure 3-1.

3.2 Loss Estimation

As to be expected, compressor performance levels are highly affected by losses in the flow path. Only the main and most significant losses in each component of the compressor are considered. Denton article, "Loss Mechanisms in Turbomachines" [1] and "Internal Flow" by Greitzer,Tan and Graf [9] have been useful in developing model for assessing losses in centrifugal compressor system flow path. Specifically the
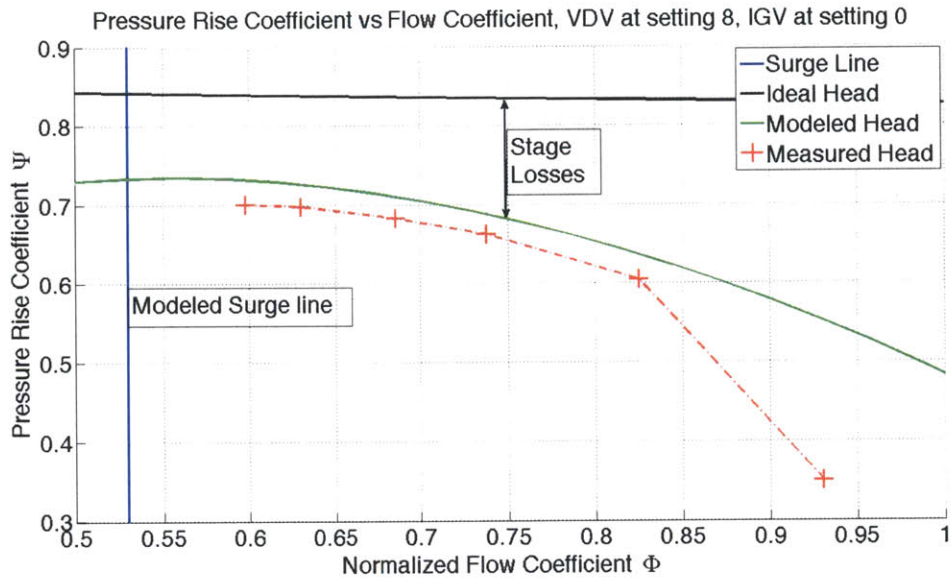
Figure 3-1: Measured and computed compressor map with nominal VDV setting and IGV setting of 0

following loss sources have been considered:

1. Skin friction

2. Shock losses

3. Mixing losses

   (a) Wake Mixing

   (b) Tip-gap losses

   (c) Losses at a blade inlet at high angle of incidence

Skin friction is only of significance when the flow has a high velocity or when the wetted surface is relatively large. It is calculated using two different models depending on the required accuracy and the assumptions made.

On the impeller blade the boundary layer characteristics are evaluated along the blade in order to calculate all the integral Boundary Layer (BL) parameters at the exit of the impeller. On every other wetted surface a more basic approach is taken. The

velocity field is approximated and a dissipation coefficient is evaluated, thus allowing loss estimation.

While shock losses are part of the model, the research compressor here is of low speed type (with subsonic flow) and the shock losses are non-existent.

3.2.1 Boundary Layer Dissipation

For incompressible flow, on each blade row (IGV & Impeller), all the integral boundary layer parameters are evaluated along the blade in order to determine the wake loss and the skin friction losses on the blades. However the velocity field outside the boundary layer has to be known in order to solve the equations. A key assumption here is that the Boundary layer shape factor $H = \delta*/\theta$ is low. Physically this means that the boundary layer does not separate. The losses are given by the following formula 3.1 as a function of the boundary layer kinetic energy thickness θ^* at each position along the blade ξ with ξ going from 0 to 1. The dissipation Φ_{BL} increases as we move along the blade surface (i.e ξ increases) because the boundary layer kinetic energy thickness increases.

$$\Phi_{BL}(\xi) = \frac{1}{2}\rho u_e^3 \theta^*(\xi) \tag{3.1}$$

The kinetic energy thickness and all the other BL parameters are found by solving the complete BL equations all along a blade [2]:

$$\frac{du}{d\xi} + (2 + H)\frac{\theta}{u}\frac{du}{d\xi} = \frac{C_f}{2} \tag{3.2}$$

$$\theta\frac{dH}{d\xi} + H^*(1 - H)\frac{\theta}{u}\frac{du}{d\xi} = 2C_d - H^*\frac{C_f}{2} \tag{3.3}$$

Solving these equations allows us to precisely evaluate all the boundary layer parameters and use them to evaluate the losses generated by the BL as detailed below.

30

3.2.2 Viscous Dissipation on Wetted Surfaces

Viscous dissipation is a major source of loss for flow with high velocity (as it scales as the relative velocity u_e^3) relative to a wetted surface (at the impeller shroud and in the diffuser). At the hub of the impeller the loss is minimal as the flow has a low relative velocity. Equation 3.4 provides an estimate of the viscous losses generated by the flow over the wetted surface. Viscous losses scale as the cube of the velocity, the area of the wetted surface and a viscous dissipation coefficient.

$$\Phi_{surface} = \rho C_D \iint_{surface} u_e^3 dS \qquad (3.4)$$

The dissipation coefficient is calculated based on guidelines given by Denton [1]. However it can be difficult to evaluate the Reynolds number in the boundary layer so a value of $C_D = 0.002$ was generally used. This is not an issue as the flow is turbulent and C_D has negligible variation for a turbulent flow as shown in figure 3-2. The boundary layer Reynolds number Re_θ typically encountered in turbomachines are above 300 and in centrifugal compressor the flow is generally turbulent. In some specific fluid region the dissipation coefficient was taken to be varying with Re_θ with $C_D = 0.0056 Re_\theta^{-1/6}$ and in that case C_D also has to be in the integral of equation 3.4.

3.2.3 Wake Mixing

Losses associated with wake mixing downstream of an airfoil are evaluated. Boundary layer analysis is carried out to determine the required boundary layer integral parameters using expression in equation 3.5 from Hall [7]. This expression is found using a control volume approach (see Figure 3-3 where the control volume is enclosed by the red dash-dot line) and using the conservation of the mass flow, the energy and the momentum of the flow. It also assumes uniform exit static pressure and uniform flow at the exit of the control volume far downstream. The static pressure drop and the mixed-out flow angle are evaluated using the following BL integral parameters that have been determined from the boundary layer flow analysis: the displacement thickness δ^* and the boundary layer momentum and kinetic energy thickness θ and

31
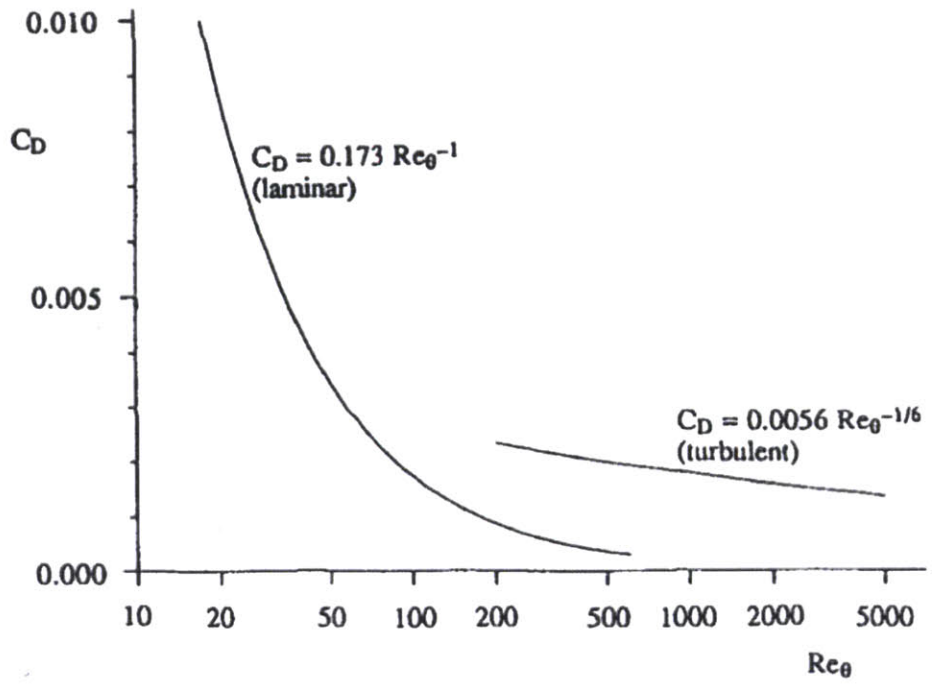
Figure 3-2: Cd for different type of flow vs BL Reynolds number from Denton[1]
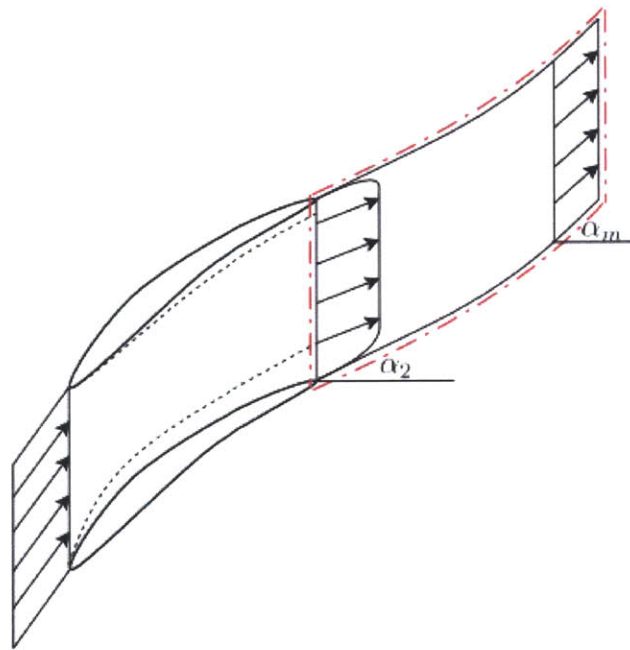
Figure 3-3: Control volume used in downstream wake mixing loss evaluation [7]

32

θ^*.

$$\frac{\Phi}{\dot{m}V_2^2} = cos^2(\alpha_2)(1 - \frac{\delta^*}{W cos(\alpha^2)})[\frac{\theta}{W cos(\alpha_2)} - (1 - \frac{\delta^*}{W cos(\alpha_2)}) + (1 - \frac{\delta^*}{W cos(\alpha_2)})^2]$$
$$+ \frac{1}{2}[1 - \frac{\delta^*}{W cos(\alpha_2)} - \frac{\theta^*}{W cos(\alpha^2)} - (\frac{cos(\alpha_2)}{\alpha_m})^2(1 - \frac{\delta^*}{W cos(\alpha_2)})^3] \quad (3.5)$$

3.2.4 Tip-gap Flow Losses

The pressure difference across the blade (arising from the high pressure on the pressure side to the low pressure on the suction side of the blade) drives a flow through the tip-gap that mixes with the main flow on the blade suction side as illustrated in Figure 3-4. The mixing out of the tip-gap flow with the main flow generates losses. The flow leaks from the pressure side to the suction side, and it is assumed to mix out
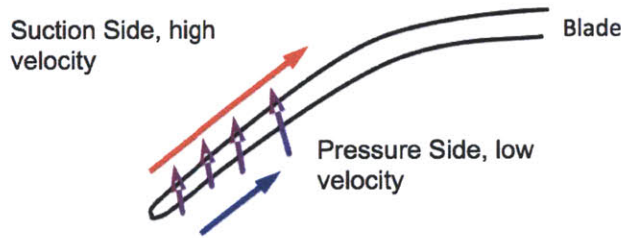
Figure 3-4: Flow leakage in a blade tip-gap

instantaneously with the flow on the suction side. Tip gap mixing loss is evaluated by assuming that the leakage flow does not modify the velocity field on the suction side. The discharge coefficient C_{diss} appearing in equation 3.6 is taken to be 0.8. The lost work is determined using equation 3.7 .

The mass flow across the gap can be calculated knowing the discharge coefficient and the pressure difference. Since the flow is assumed incompressible the pressure difference across the gap can be calculated knowing the velocity on the suction and pressure side and we get equation 3.6 for the efficiency penalty associated with the

tip-gap flow.

$$\Delta \eta_{gap} = \frac{\Phi_{gap}}{\dot{m}V_2^2} \frac{\Phi^2}{\Psi} = C_{diss} \frac{\tau}{h} \frac{C_s}{c} \frac{\phi}{\psi} \sigma \int_0^1 \frac{U_{ss}}{U_2} (\frac{U_{ss}}{U_2} - \frac{U_{ps}}{U_2}) dl \qquad (3.6)$$

In chapter 6 & 7 when this loss is calculated using CFD no assumption is made and the loss is directly calculated using the following equation that is integrated along the surface of the tip-gap:

$$Td(S_{tip-gap}) = V_s^2 \left(1 - \frac{V_p}{V_s}\right) \frac{dm}{m_m} \qquad (3.7)$$

3.2.5   Slip at Impeller Tip

The flow does not leave the impeller parallel to the blades, as one would expect. Because of the Kutta condition, there is no pressure difference at the blade trailing edge. This difference of pressure across the blade has to gradually reduce to a vanishing value at the trailing edge. Therefore the flow does not follow the blade direction anymore since it has to satisfy to the Kutta condition, and is inclined backwards as seen in figure 3-5. This is characterized by a slip factor that reduces the achievable head pressure rise.

Using Wiesner definition based on Stodola calculation on slip velocity [5] we evaluate the slip factor σ using the number of blades N and the blade metal angle χ_2 at the impeller exit:

$$\sigma = 1 - \frac{\pi}{N} cos(\chi_2) = 1 - \frac{V_{slip}}{U_2} \qquad (3.8)$$

We now evaluate the new absolute tangential velocity at the exit of the impeller.

$$V_{\theta 2} = V_{\theta 2 ideal} - V_{slip} \qquad (3.9)$$

And we obtain, with U_2 the impeller tip speed and V_n the meridional flow speed:

$$V_{\theta 2} = U_2 - V_n tan(\chi_2) - U_2(1 - \sigma) \qquad (3.10)$$

34
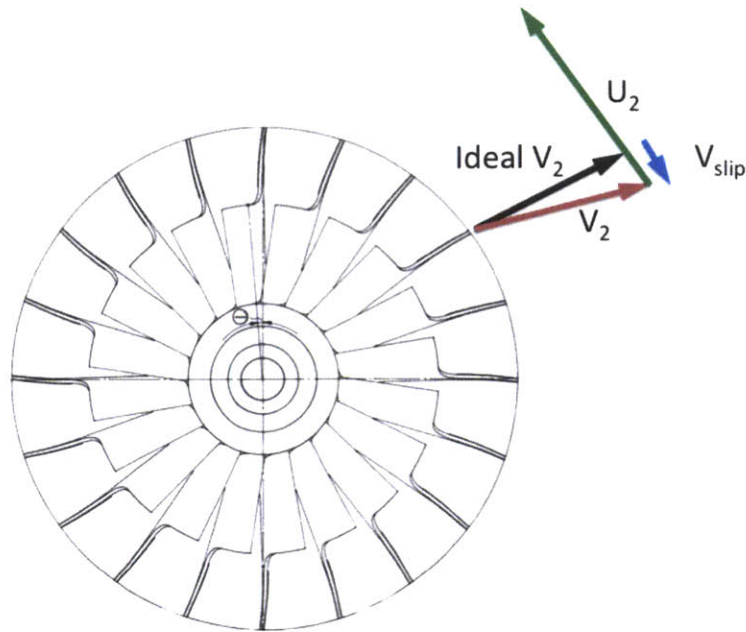
Figure 3-5: Impeller Slip, Slip vector in blue, impeller tip speed in green, ideal velocity vector in black, real velocity vector in red

3.2.6 Loss due to High angle of Incidence

When the IGV or diffuser has a high angle of incidence $(\beta - \chi)$ with β the relative flow angle in the blade reference frame and χ the blade metal angle, the flow detaches resulting in unacceptable high losses. If the extent of flow separation can be estimated then the loss may be calculated by evaluating the loss associated with the mixing out of the separated regions. In view of this it was assumed that the kinetic energy of the flow created by the velocity component normal to the blade metal angle is entirely dissipated and the associated loss was determined.

3.2.7 Shock Losses

The flow can be transonic or even supersonic in the diffuser. As a consequence shock losses arise. Such losses are minimal if the Mach number is in the order of 1.

The losses in the diffuser are highly dependent on the blade solidity. High solidity blades form a channel of smaller area with higher Mach number. For the flow situations encountered here, the diffuser flow is entirely subsonic so there are no loss
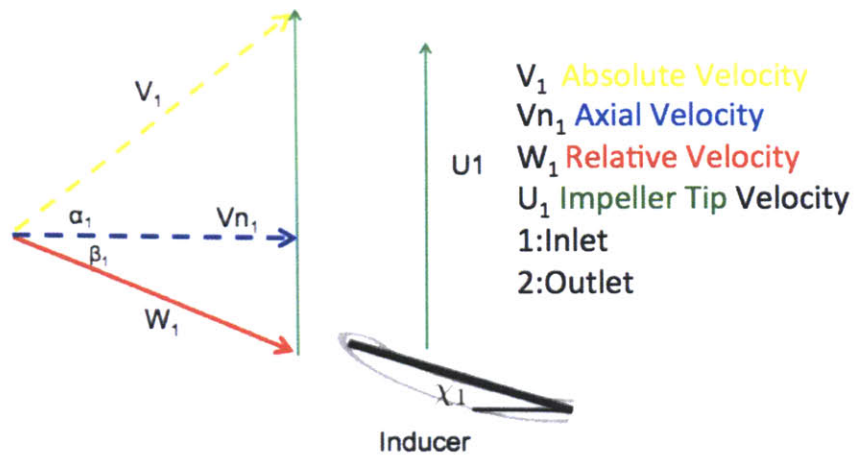
Figure 3-6: Velocity triangle at impeller entrance

associated with shock.

3.3 Components Model

The compressor flow path can be viewed to consist of four main sections as seen in figure 3-7, each with its own loss sources:
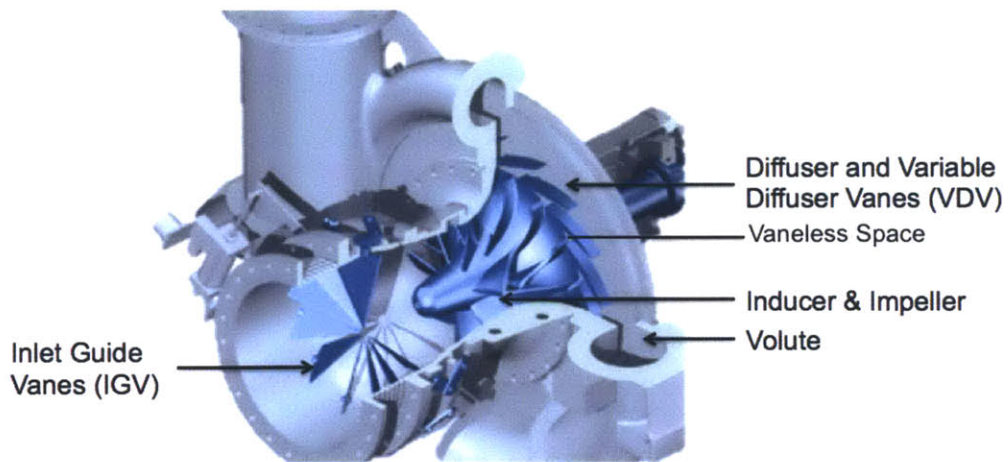
Figure 3-7: Compressor's components

- Inlet Guide Vanes

- Impeller

- Vaneless space

- Variable Diffuser Vanes

- Volute

The overall compressor effective head is found by multiplying each component's isentropic efficiency with the ideal head.

$$\Psi_{effective} = (\prod_i \eta_i)\Psi_{ideal} \tag{3.11}$$

3.3.1 Impeller Model

Assumptions

The flow is assumed to be at steady-state and there are no variations from hub to shroud, it is further assumed that such a flow can be used to represent the flow along the mean-line, hence the mean-line model.

The flow in the impeller passage is taken to be incompressible; this will limit the validity of the model to low pressure ratio subsonic machines. To justify this we first evaluate the following characteristics quantities:

In a rotating impeller, we have:

$$\Delta p \sim \rho \Omega^2 r^2 \frac{\Delta r}{r} \tag{3.12}$$

The flow can be taken to be incompressible if:

$$\frac{\Delta p}{p} << 1 \tag{3.13}$$

We define the rotational Mach number:

$$M_\Omega = \frac{\Omega r}{a} \tag{3.14}$$

Using the above criteria we find the flow can be approximated as incompressible if:

$$M_\Omega^2 \frac{\Delta r}{r} << 1 \qquad (3.15)$$

For the situation here:

$$M_\Omega^2 \frac{\Delta r}{r} = 0.2 \qquad (3.16)$$

Thus the flow can be approximated as incompressible in the impeller.

For the type of Centrifugal compressor considered we have:

$$\frac{A_{out}}{A_{in}} \approx 0.92 \qquad (3.17)$$

Thus we can approximate the meridional velocity at the inlet (1) and outlet (2) to be equal $V_{n1} \approx V_{n2}$ as the density varies little across the impeller. The meridional velocity at the impeller inlet is taken to be the same as the meridional velocity at the outlet of the impeller.

The flow is also assumed to be steady and inviscid, however viscous losses on wetted surfaces are computed.

An Ideal Meanline Model

We use the Euler turbine equation to determine the change of stagnation enthalpy per unit mass Δh_t and we express the exit tangential velocity as a function of the impeller backsweep angle, the tip speed and the flow normal velocity.

We then express the flow inlet velocity as a function of the inducer angle and the normal velocity at the inducer inlet.

The stagnation enthalpy rise can be computed, with station 1 being the inlet and station 2 the outlet as seen on Figure 3-8, R the radius at the inlet (1) / outlet (2), and V_n the meridional velocity. V_n is the velocity component normal to the inlet (1)
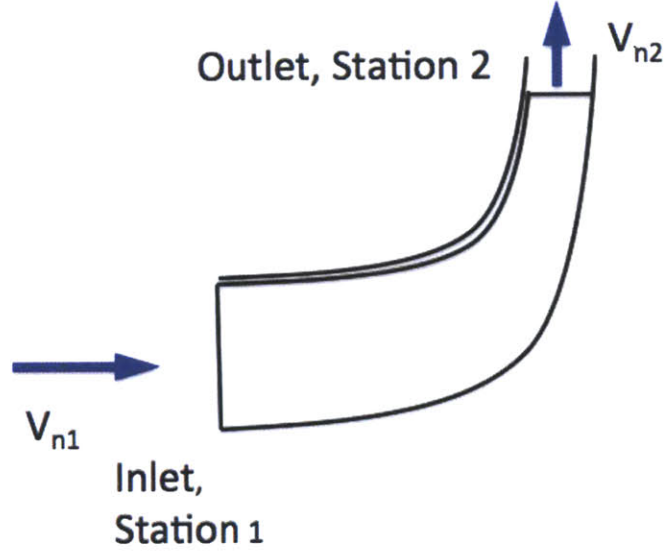
Figure 3-8: Impeller schematic with the station numbers

/ outlet (2) areas, in our case it is the meridional velocity.

$$\frac{\Delta h_t}{U_2^2} = 1 - \frac{V_{n2}}{U_2}\tan(\chi_2) + \frac{R_1}{R_2}\frac{V_{n1}}{U_2}\tan(\alpha_1) \qquad (3.18)$$

We use the following non dimensional aerodynamic characteristic parameters.

- The stage loading/head coefficient: $\psi = \frac{\Delta h}{U_2^2}$

- The flow coefficient: $\phi = \frac{V_{n2}}{U_2}$

For impeller where the exit cross-section area differs from the inlet one, V_{n1} is different from V_{n2}. By relating the exit and inlet velocity using a compression polytropic efficiency η_p we find, starting with the Euler Turbine equation:

$$\psi + \tan(\alpha_1)(\frac{2R_2 d_2}{R_1^2})\phi(\frac{\gamma-1}{\gamma\eta_p}\frac{U_2^2}{RT_1} + 1)^{\frac{\gamma\eta_p}{\gamma-1}+1} = 1 - \phi(tan(\chi_2)) \qquad (3.19)$$

Adding the impeller reduced head due to the slip factor (which is an inviscid effect) we obtain:

$$\psi + \tan(\alpha_1)(\frac{2R_2 d_2}{R_1^2})\phi(\frac{\gamma-1}{\gamma\eta_p}\frac{U_2^2}{RT_1} + 1)^{\frac{\gamma\eta_p}{\gamma-1}+1} = \sigma - \phi(\sigma tan(\chi_2)) \qquad (3.20)$$

Since the flow is approximated as incompressible, and the exit area is approximately similar to the inlet area of the impeller: $V_{n2} \approx V_{n1}$. Equation (3.20) simplifies to:

$$\psi = \sigma - \phi(\sigma tan(\chi_2) + \frac{R_1}{R_2} tan(\alpha_1))$$ (3.21)

The ideal pressure rise for an inviscid flow is computed with Euler's turbine equation:

$$\frac{\Delta P_t}{\rho} = \omega \Delta(rV_\theta)$$ (3.22)

Velocity profile

In order to evaluate the losses in the impeller all the integral boundary layer parameters have to be evaluated. To do so we must first estimate the average velocity field on the impeller blades. The boundary layer parameters are computed using a Matlab code based on the use of Drela's expressions for the growth of a boundary layer [2]. The organization of the code is presented in Figure 3-9.

Inputs:
- Surfaces and dimensions
- Velocity profile
- BL equation

Solver:
- Incompressible
- Turbulent Flow
- Newton method
- Turbulent closure

Results:
- All the BL parameters (thickness, velocity profile,...)

Post-treatment:
- Blade surface dissipation
- Wall dissipation
- Tip leakage
- Wake mixing
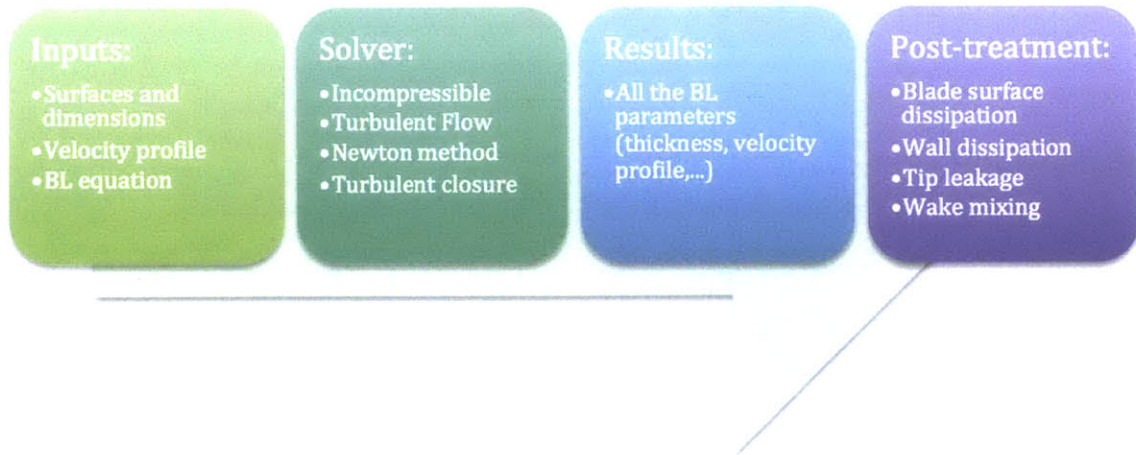
Figure 3-9: Organization of the boundary layer code

Several velocity profiles have been measured on impellers. If we average the ve-

locity at the hub and at the shroud, these velocity profiles were found to be approximately rectangular. This is especially true for impeller with low backswept angle as illustrated in Figure 3-11. It was decided to use a rectangular velocity profile to approximate the velocity distribution on the impeller blades.

As seen in figure 3-12, four quatities have to be evaluated: the inlet velocity V_1, the exit velocity V_2, the mean velocity $\bar{V}$, the velocity difference between the suction and the pressure side of a blade ΔV and the mean velocity. The inlet speed V_1 and the exit speed V_2 are calculated using mass conservation in conjunction with the impeller blade angle. ϕ is the flow coeficient V_n/U_2 and ψ is the head coefficient.

$$V_n = V_1 cos(\alpha_{in}) = V_2 cos(\alpha_{out}) = U_2 \phi cos(\alpha_{out}) \tag{3.23}$$

The average velocity is calculated using the stagger angle ξ, and the ratio of meridional blade surface length c_s divided by the blade chord c as seen in Figure 3-10. Equation 3.24 is obtained by comparing the change of angular momentum of the flow to the change of pressure across the blade.
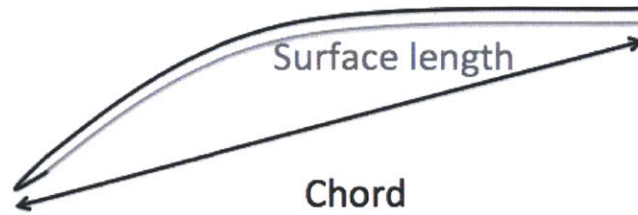
Figure 3-10: Comparison of the Chord and the surface length

$$\bar{V} = \frac{c_s}{c} \frac{V_n}{cos(\xi)} \tag{3.24}$$

The velocity jump at the leading edge is evaluated by matching the amount of turning through the passage to the circulation around a blade, with σ the blade solidity.

41

$$\Delta V = \frac{V_n}{\sigma(c_s/c)} \frac{\psi}{\phi} \tag{3.25}$$

DESIGN-POINT IMPELLER BLADE SURFACE VELOCITY DISTRIBUTION
MEDIUM PRESSURE RATIO IMPELLER (SHROUD—— AND HUB--- STREAMTUBE
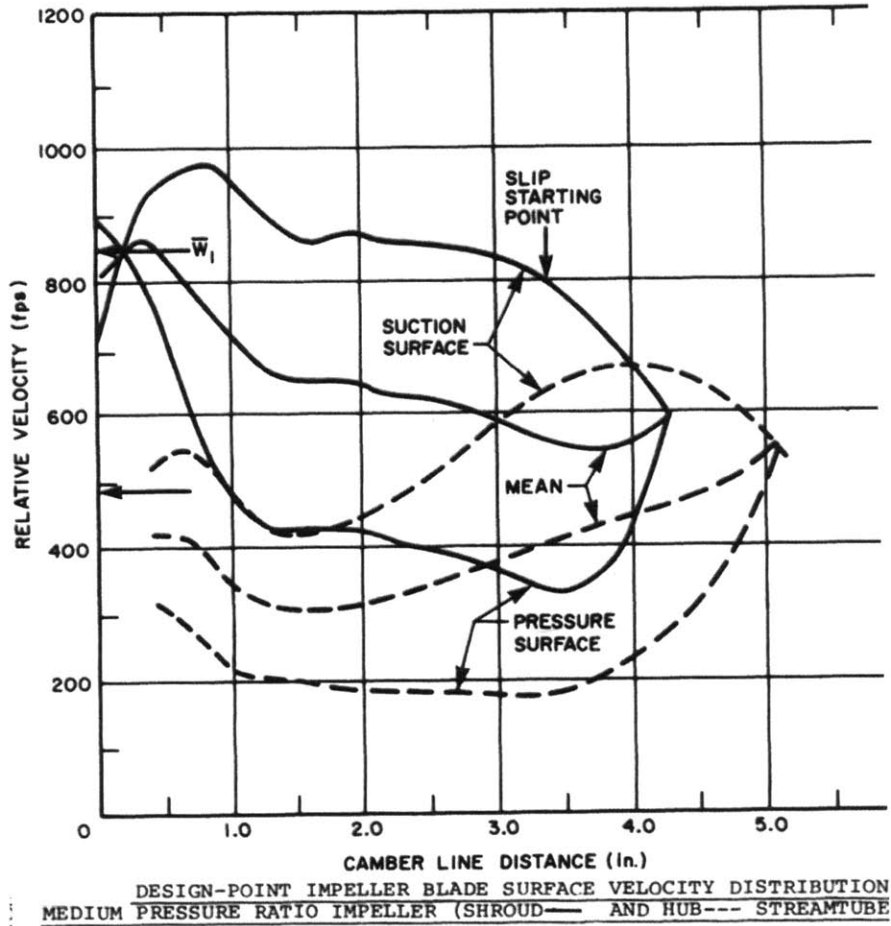
Figure 3-11: Impeller blade surface velocity distribution [15]

Impeller losses

The surface dissipation on the blade is estimated in accordance with the solution of equations 3.2 and 3.3. The wake dissipation is evaluated with equation 3.5. At the same time a simpler and more direct approach is used to evaluate the surface dissipation on the hub and on the shroud, they are computed using equation 3.4. The tip leakage loss is estimated with equation 3.6.

42
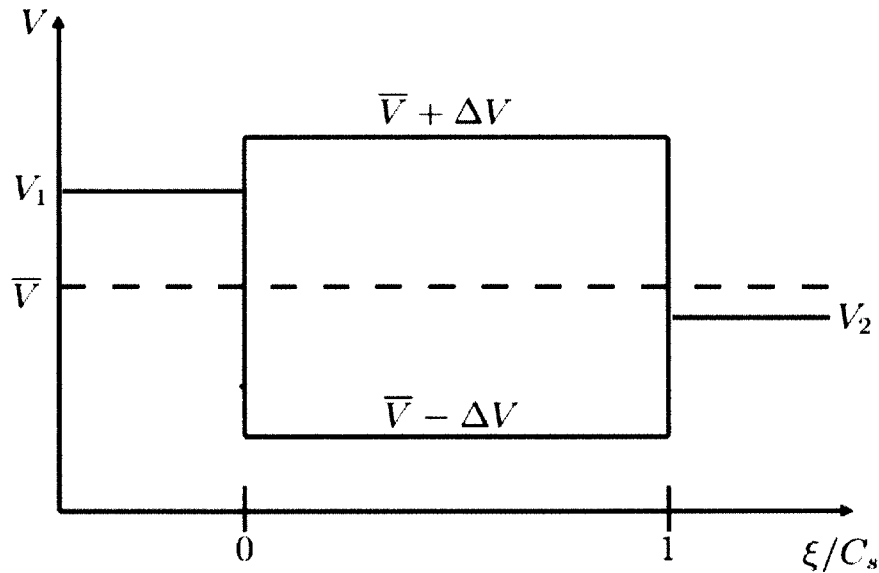
Figure 3-12: Typical rectangular surface velocity distribution approximation on an impeller blade

Using the equations presented above, the losses from the impeller and the effective head can be evaluated.

It is found that for low flow coefficient the loss of efficiency has a steep drop. Low flow coefficient means high flow angle, so the flows travels a much longer path (i.e. helical trajectory with a shorter pitch). The flow angle α is roughly $1/\phi$. So frictional loss at the shroud can be expected to increases greatly at low flow coefficients. In other words, the flow perceives a larger surface area with a resulting increase in dissipation loss as seen in figure 3-13. The model used here underestimates the wake losses, this is probably because it is assumed that the boundary layer does not separate.

3.3.2 Inlet Guide Vanes

The Boundary Layer model used in the impeller is used in the IGV for low IGV angle. The IGV has an efficiency penalty that rises with the average flow velocity at the entrance so it increases with the flow coefficient. However at high angle the efficiency penalty is large because the flow detaches and the impact on the total pressure loss can be significant. This is not modelled as it is assume that the machine

43
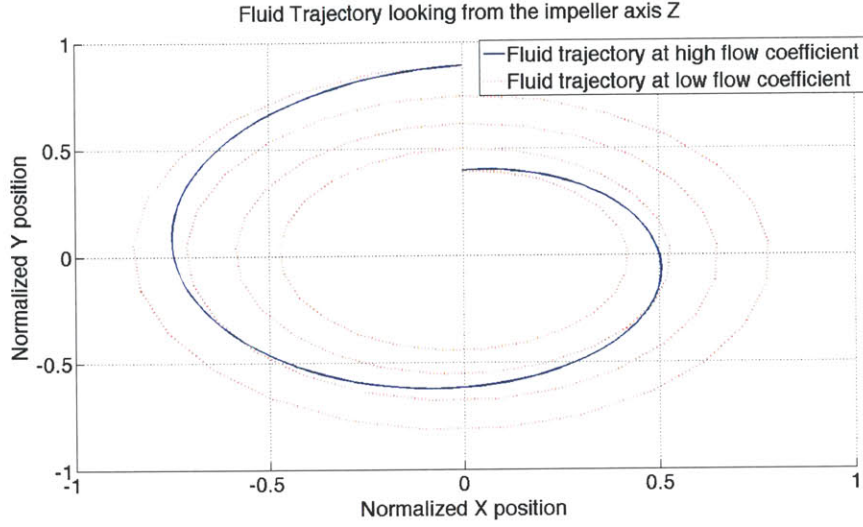
Figure 3-13: Projected fluid particle trajectory at different flow coefficient

will not be used at unacceptably high IGV angles (low IGV setting) but rather that the rotational speed will be reduced.

3.3.3 Vaneless Space

The flow in the vaneless space can have a Mach number close to unity. However to estimate the loss generated in the vaneless space, the flow is approximated as incompressible. This is reasonable as $\frac{\Delta r}{R_{impeller}} \approx 0.1$, with Δr the change of radius in the vaneless space and $R_{impeller}$ the impeller exit radius, so the change of pressure is small. Also for absolute flow angles above $60°$ at the impeller exit (which is the case here), and for a flow that has an initial Mach number of about 0.6 which is the case here, the change of flow angle due to compressibility is small. Its value can be calculated with equation 3.26 and 3.27 [9]. It is found that in this situation $\Delta \alpha < 3°$, the swirl angle does not vary significantly. A constant flow angle can be assumed. Both the radial and the tangential velocity decay as $\frac{1}{r}$ according to the mass flow equation and the constant angular momentum of the flow.

$$\frac{dM^2}{M^2} = \frac{-2(1 + (\gamma - 1)M^2/2)}{1 - M_r^2} \frac{dr}{r} \qquad (3.26)$$

44

$$da = \frac{-(M^2 sin2\alpha)}{2(1 - M_r^2)} \frac{dr}{r} \qquad (3.27)$$

The loss is evaluated using the same skin friction formula as used in the impeller:

$$\eta_{vaneless} = 1 - \frac{\Phi_{vaneless}}{\dot{m}\Delta h} = \frac{\rho C_d}{\dot{m}\Delta h} \iint_{surface} u_e^3 dS \qquad (3.28)$$

The efficiency penalty due to the vaneless gap can be substantial at low flow coefficient. Low flow coefficient means a low flow angle. So the flow travels in spiral with a short pitch with a consequence of a perceived large wetted surface area as seen in Figure 3-13.

3.3.4   Diffuser
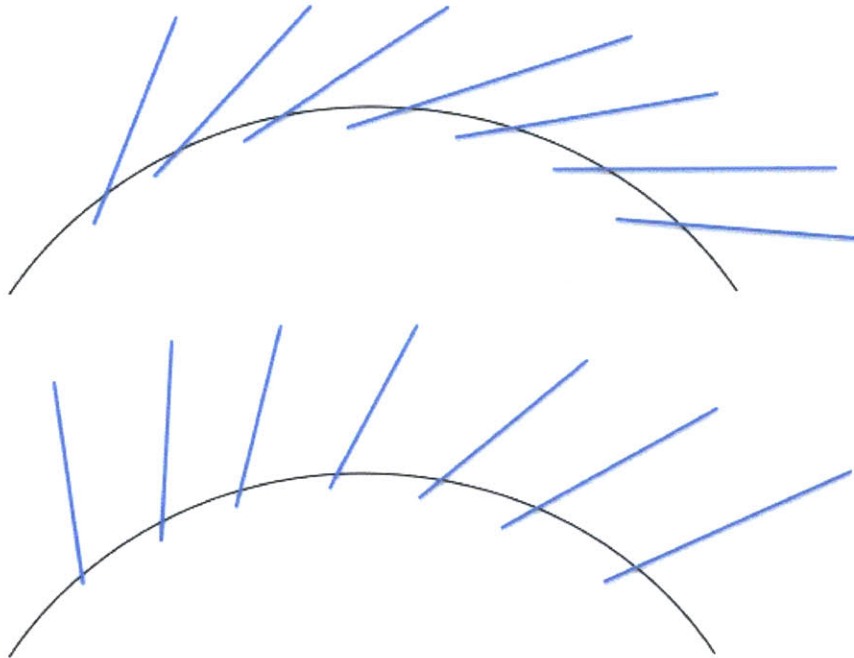
Figure 3-14: Different diffuser geometry for small (above) and large (below) VDV settings

The flow in the diffuser is complex and several assumptions have to be made. While the flow is compressible in the diffuser, it is being approximated as an incom-

45

pressible flow here. However an average value of the density is used. This allows the diffuser to be modelled in a similar way as the impeller. The diffuser blade surface velocity profile is assumed to be triangular. However the velocity profile varies with the diffuser blades setting angle as seen in Figure 3-14. The BL equations are not solved and the losses are evaluating directly by integrating the velocity field over the wetted surface using an appropriate dissipation coefficient. Mixing losses at the diffuser inlet is determined as follow. It is known that losses increase significantly when the incidence angle of the blade with the flow increases as illustrated in figure 3-15. The component of the kinetic energy of the flow due to the velocity perpendicular to the metal blade angle is assumed to be entirely dissipates into losses.

The tip-gap losses are also calculated since the velocity on both suction side and pressure side is known.
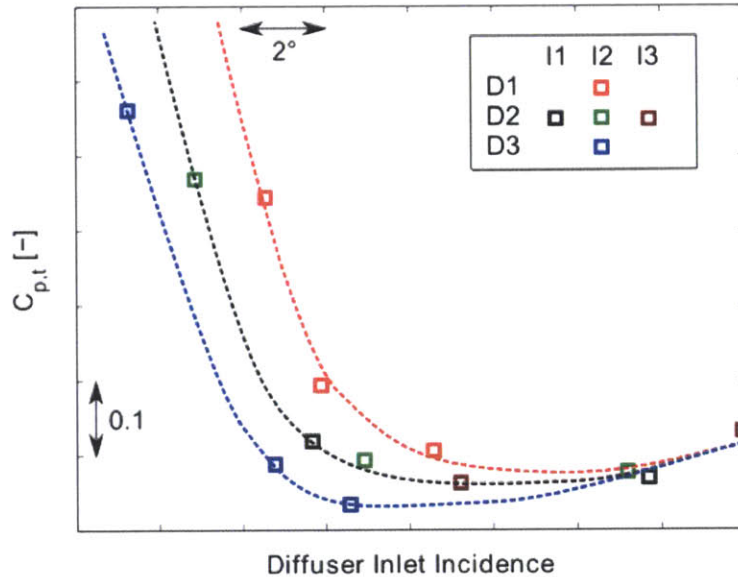
Figure 3-15: Losses at the diffuser inlet as characterized by Everitt [8]

3.3.5 Volute

The flow is assumed to leave the diffuser vanes at the metal blade angle. In the volute the flow is assumed to be purely tangential and has no radial component. Since there
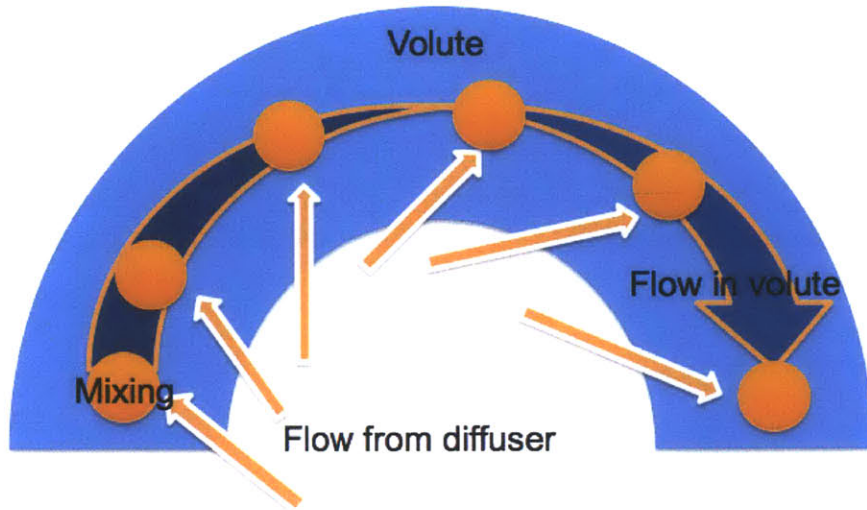
Figure 3-16: Mixing out of the flow in the volute

is an increase of radius between the VDV and the volute the new flow angle at a radius right before the volute is calculated using the conservation of angular momentum. It is then assumed than any component of the kinetic energy due to the radial velocity of the incoming flow in the volute will be dissipated as a loss as seen in figure 3-16. To evaluate this loss source, the mass flow in the volute is assumed to vary linearly from beginning of the volute to the tongue. The mass flow distribution in the volute is varying tangentially as more flow from the diffuser is injected into it. The exact flow in the volute is calculated knowing the area at any angular section and is assumed to be a function of the angular coordinate θ only (1D flow). Figure 3-16 illustrate how the flow coming from each diffuser vane is injected and mixes-out in the main flow of the volute.

$$\Phi_{volute} = \frac{d\dot{m}}{2\dot{m}}((u_x - u_{x_{inj}})^2 + u_{y_{inj}}^2) \tag{3.29}$$

3.4   Surge Criteria and Exit Conditions

It is of great importance to determine the surge line in the compressor map and to be able to evaluate its dependence on other parameters. It was decided to use the surge

criteria given by Cumpsty [5]. The stability parameter SP is defined as:

$$\sum_i SP_i = \sum_i \frac{1}{PR_i} \frac{\partial PR_i}{\partial m_i} \leq 0 \tag{3.30}$$

As seen on Figure 3-17, the surge point occurs when the total SP becomes negative. It is also clear that the impeller and the volute have a destabilizing effect while the vaneless space has a stabilizing one. The diffuser is the key component here as it is the one that has the largest negative slope. Therefore the surge point can be highly dependent on the diffuser design.
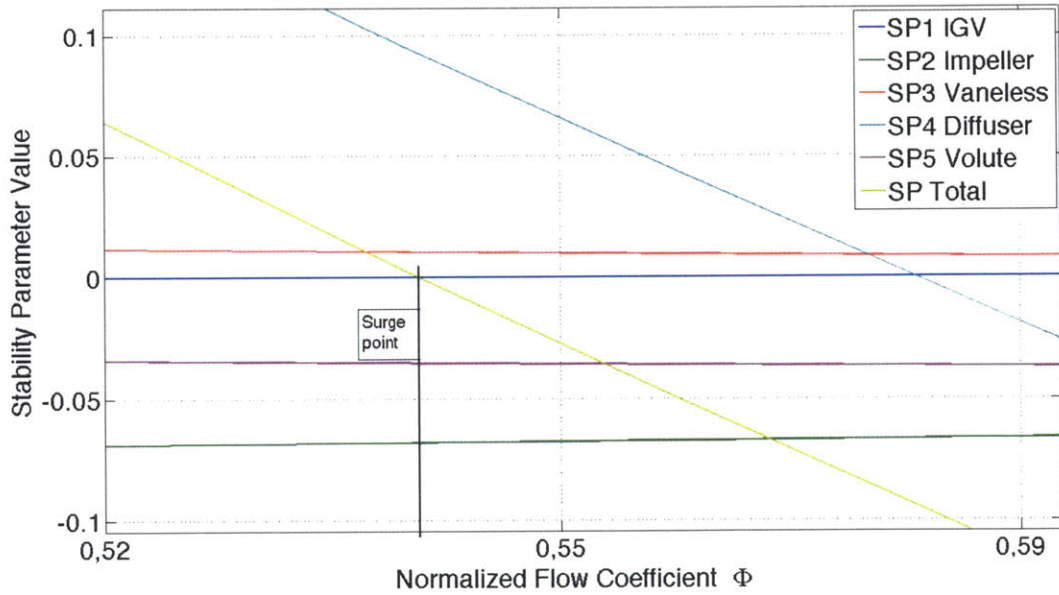
Figure 3-17: Stability Parameter of each component and total SP

The mass flow of the compressor was calculated assuming downstream exit conditions are known. It is found by calculated the intersection of the throttle line and the theoretical mass flow curve that depends on the total pressure generated by the machine.

3.5 Summary

This chapter describes the formulation and development of the mean-line model for estimating the performance of centrifugal compressor. This model incorporates loss estimation for the IGV, the impeller, the vaneless space, the VDV and the volute. The loss estimation requires the knowledge of boundary layer integral parameters, dissipation coefficient, discharge coefficient and the velocity field around an impeller blade. The estimated performance is in agreement with the measured one as illustrated in the following chapter.

Chapter 4

Formulation of a Control Framework

4.1 Introduction

In this section results from the meanline model described in Chapter 3 are presented. The influence of the IGV, the VDV and the RPM on the computed performance is evaluated. The surge criterion is also assessed against available data. The model is then used to establish a control framework to optimize the compressor system at any working point and during the transition between two working point.

4.2 Mean-line model Results

Using the mean-line model developed in the previous chapter, the compressor map for any set of angle can be determined and evaluated.

4.2.1 Effect of the IGV

The IGV is used both to reduce the head and to achieve lower mass flows without surging or stalling. As explained previously the model is accurate enough for IGV angles up to about 30 degrees. For higher angle the IGV induces substantial losses and
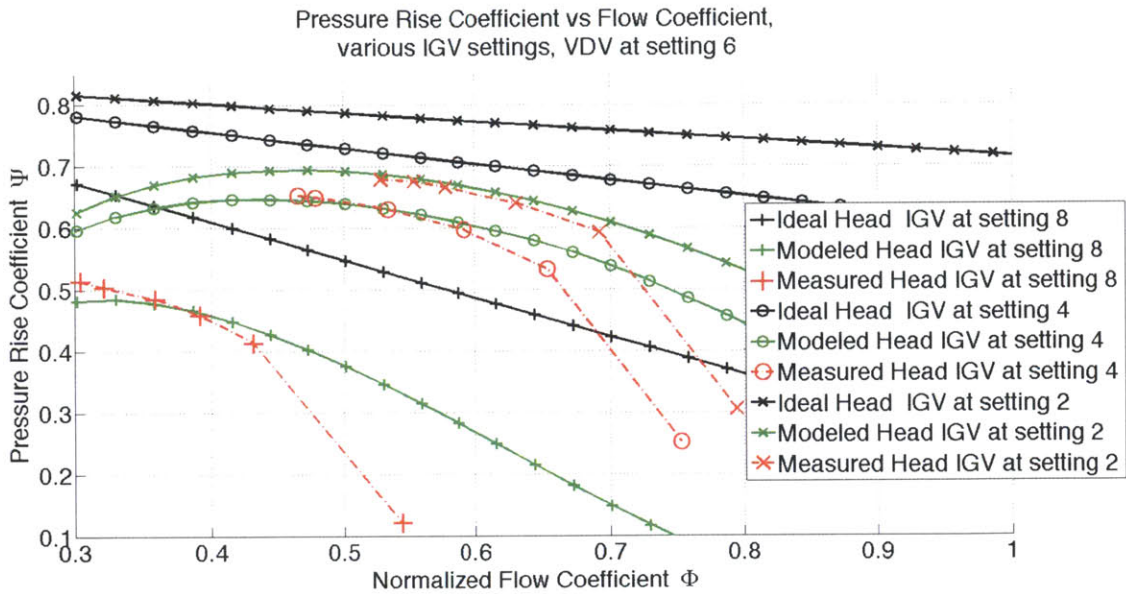
Figure 4-1: Computed compressor characteristic with VDV set at setting 5 and various IGV settings

the machine efficiency drops sharply as illustrated in Figure 1-2 . For IGV settings between 4 and 10 the efficiency of the machine has a weak functional dependence on the IGV angle and the IGV are then effective in reducing the pressure rise coefficient . As see in Figure 4-1 the minimal flow coefficient is reduced by 40% and the head drops by 15% when going from setting 8 to setting 2, this corresponds to an increase in swirl of 30°.

4.2.2 Effect of the VDV

The VDV is changed by 10° when going from setting 4 to setting 10. Over that range the maximum head does not vary significantly but the minimum flow coefficient drops by 35%. For setting 6, the VDV has a more radial angle setting than setting 3. The measured head for a VDV setting of 10 is lower than the measured head for a VDV setting of 8 for normalized flow coefficient below 0.75. The model also captures this effect but the flow coefficient where that intersection occurs is 0.61. The lower head achieved is explained by the large angle of incidence of the flow makes with the vanes, and it becomes beneficial efficiency wise to use large VDV setting (diffuser passage
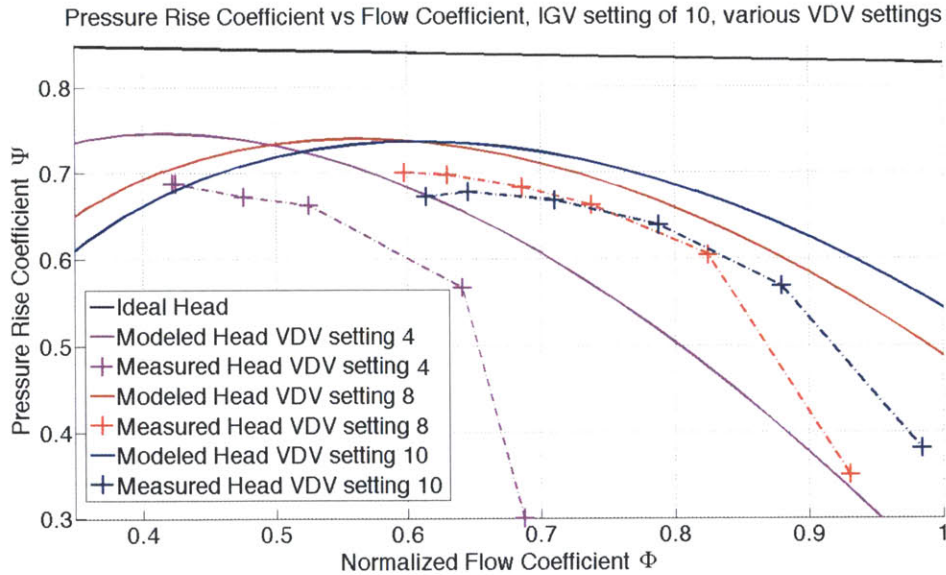
Figure 4-2: Simulated compressor with no IGV angle and various VDV angles

more open, vanes closer to the radial axis) only when the flow coefficient is large enough. For large flow coefficient the flow has a more radial trajectory and the angle of incidence with the diffuser blades is minimal.

The losses due to the angle of incidence of the flow with the VDV scales as $(V_m sin(\alpha))^2$ with V_m the meridional velocity at the diffuser inlet and α the angle of incidence of the flow on the diffuser blades. As noted in Chapter three it was assumed that the kinetic energy of the flow created by the velocity normal to the blades is dissipated.

As seen from the results in Figure 4-2, the ideal head from Euler turbine equation is the same for all VDV settings (black line), unlike the IGV, the diffuser vanes cannot be used to efficiently reduce the head achieved by the flow and can only be used to match the diffuser to a specific flow coefficient, thus improving the efficiency of the compressor.

4.2.3 Effect of the Impeller Speed

The Impeller speed has almost no effect on the non-dimensionalized head rise as it is non dimentionalized by the impeller tip-speed as seen on Figure 4-3. However some

losses are also a function of the impeller speed, as the velocity distribution of the flow around the impeller and diffuser blades is modified when changing the impeller speed. However this is a small effect and as long as the diffuser remains subsonic the effect of the impeller speed on the non-dimensionalized head can be ignored.

The impeller speed can have a significant effect on the total pressure rise and the mass flow. It is used in conjunction with the vanes angle in the control framework to adjust the mass flow and the pressure ratio of the rig to match the required values requested by the customer.
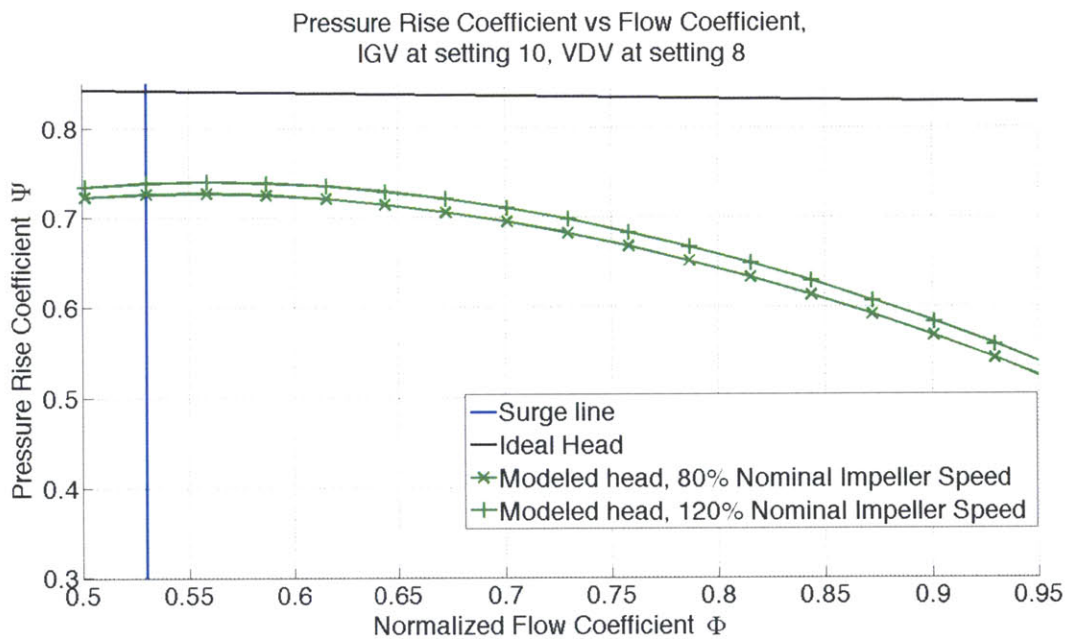
Figure 4-3: Computed compressor characteristics with no IGV angle but with VDV at setting 8 and various impeller speed

4.2.4 Surge line

The surge line measured experimentally was compared to the one computed using the surge criteria given by Cumpsty [5]. As see in table 4.1 the computed surge line trends and variations are in accord, but the absolute values cannot be reliably used throughout the compressor operating range. It is safer to use the surge point measured experimentally, but for design purposes the surge criteria can be used as

guideline since the qualitative trend is in accord with data.

Table 4.1: Normalized Flow Coefficient surge point for different IGV settings and a VDV setting of 6

IGV setting	2	4	6	8	10
Measured surge point	0.30	0.43	0.46	0.52	0.57
Modeled surge point	0.30	0.38	0.41	0.44	0.47
Relative error in %	0	12	11	15	18

4.3 Performance Metric

A control framework can either be formulated during the design process of the compressor or it can be implemented after a compressor system has been built. In our case the control framework is implemented to conform to the requirements of the existing compressor system. Its goal is to minimize the power consumption while still satisfying the customer requirement in terms of flow rate and exit pressure. The overall complete system efficiency is used to develop the control framework. It takes into account all the losses at all the levels, including non fluid related losses associated with the operation of the gears and the motor.

The current model includes a typical industrial gear efficiency and a typical electrical motor efficiency. The gear efficiency curve is assumed to be linear and the electrical motor is also assumed to have a linear efficiency. This is usually true for the electrical motor if the power stays above 30 to 40% of its maximum rated value. If the compressor is to be powered by a turbine the formulated model is flexible and the turbine efficiency characteristics can replace the electrical motor characteristics. The goal here is not to maximize the compressor efficiency but to minimize the total amount of energy used by the customer.

The turndown (or minimum flow coefficient that can be attained without surging) is the other key metric. Since it is assumed the compressor system configuration is

already determined and that it is operational, no geometrical parameters are used as inputs for the control algorithm.

4.4   Formulation of a Simple Control Framework

A control system allows the compressor system to work at its highest efficiency for any working point. The control framework is based on the three following control variables:

1. The Inlet Guide Vanes (IGV) angle setting can be used to add swirl to the flow thus reducing the head achievable by the system. One of the other key effects of the IGV is that increasing IGV angle also increases the turndown and improves stall margins. At very high IGV angle the efficiency of the system drops.

2. The Variable Diffuser Vanes (VDV) are used to match the diffuser to the flow at any flow coefficient. The turndown is the main metric affected by a change of VDV angle. The head can only decrease and the efficiency lowered if the VDV are not adjusted appropriately.

3. The Impeller speed (RPM) can also be adjusted to change the flow coefficient or the head achieved by the system.

By using the meanline model, the control frameworks simulates the desired working conditions and the losses occuring in the system. It then picks the best set of values for the 3 parameters IGV setting angle,VDV setting angle and impeller speed to accommodate the specified requirements.

4.5   System Optimization

Two types of optimization algorithm have been developed. One that can adjust the diffuser vanes and one where those vanes are fixed. The algorithms are different as explained in the following.

4.5.1 Control With Adjustable Diffuser Vanes

The Control framework requires the user to select a desirable flow coefficient (or mass flow) and the exit pressure. It then outputs the values of the IGV and VDV setting and impeller speed corresponding to the required head rise while maximizing the efficiency. The algorithm works in 5 main steps:

1. Eliminate all the set of solutions that are not in the operable range, i.e the operating points corresponding to regimes beyond surge or choking

2. Evaluate the compression efficiency for each of the remaining solutions

3. Adjust the impeller speed to match the required output pressure

4. Calculate the system losses that are a function of the RPM (electrical motor and gear)

5. Evaluate the total efficiency of the system for the remaining solutions

6. Pick the best solution with the highest system efficiency

The formulated approach is based on the results of the mean-line model. First the control model seeks out the desirable operable space so that a pre-schedule variation of operating point stays within the operational space. The optimal working point is evaluated and selected, maximizing the efficiency of the system. The procedure is detailed in Figure 4-4. In terms of practical implementation, the pre-schedule position and the operable space can be coded in a computer program module for implementation in the controller for the compressor system. This allows the controller to always select the right working point without having to run the full mean-line model.

4.5.2 Control Without Adjustable Diffuser Vanes

If there are no adjustable diffuser vanes, the algorithm is different as the only variables left are the IGV angle setting and the impeller speed. The procedure is detailed
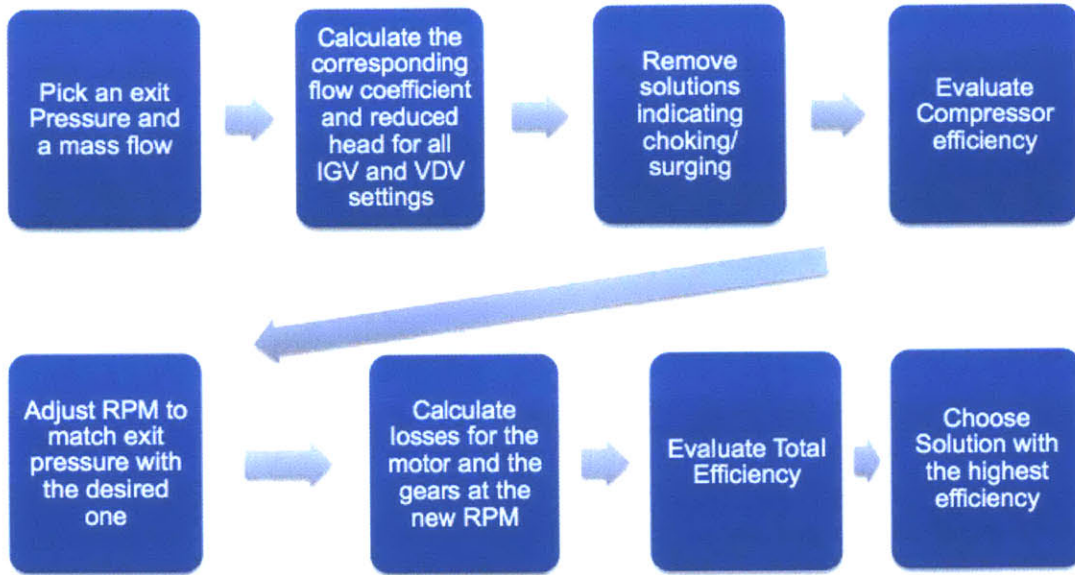
Figure 4-4: Algorithm steps with adjustable vanes

in Figure 4-5. Removing the VDV angle setting as a variable adds constrain on the space of solutions as the diffuser vane angle is now fixed, and that fixed angle has to be the optimal compromise for all the desirable working points. A cost function is defined in order to evaluate that optimal compromise. Maximizing that cost function allows us to solve the value of the fixed diffuser vane angle and the averaged efficiency.

The cost function is the sum of the product of the evaluated factor times the system efficiency for each flow coefficient. The evaluated factor is the relative importance of each working point (flow coefficient) and is given by the customer. It is the normalized amount of time the compressor is expected to be used at that flow coefficient. In other words, the cost function is a weighted average of the different efficiencies at each flow coefficient.

T_{VDV} is a parametric cost function. The variables are the impeller speed and the IGV setting angle, and the parameter is the diffuser vane angle.

$$T_{VDV} = \sum_i Ef(\phi_i).\eta(\phi_i) \tag{4.1}$$

57
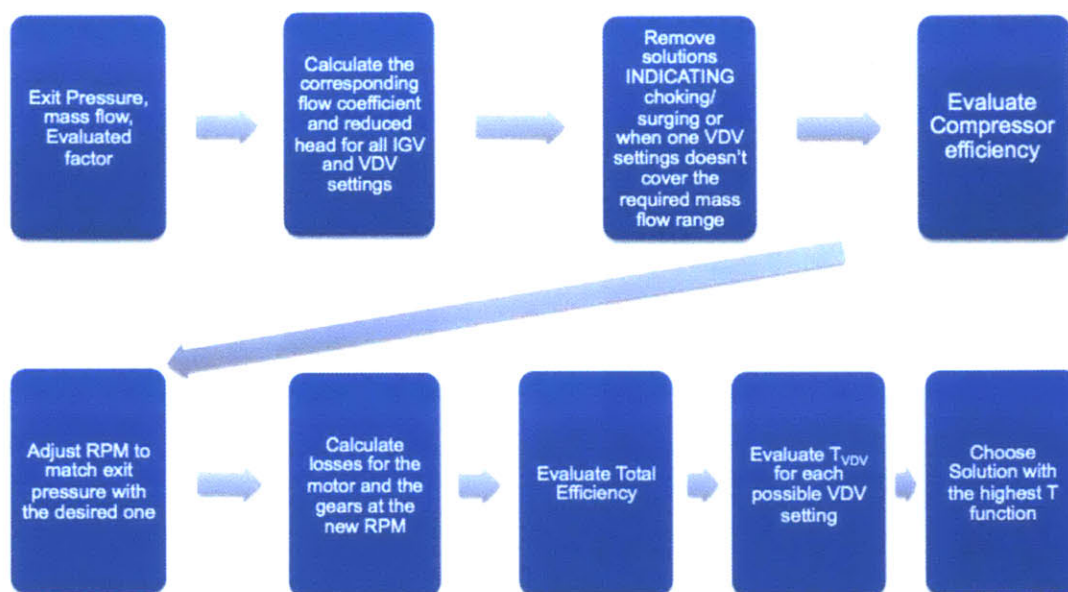
Figure 4-5: Algorithm steps without adjustable diffuser vanes

When T_{VDV} is at its maximum, it implies that for each working point the best impeller speed and IGV setting angle are selected so that the diffuser vane angle is optimal for all working points. It does not necessarily mean that each working point has the maximum efficiency possible; only the weighted averaged value is maximized. Since the diffuser is not adjustable, the turndown of the machine is higher (it is not possible to reduce the mass flow as much as with adjustable diffuser vanes) so the usable safe range of flow is smaller. Typically a drop of efficiency of 5 points was observed if the diffuser vanes are fixed compare to a machine with variable diffuser vanes. The compressor has to work inefficiently at the lowest and highest required mass flow. For a compressor with adjustable diffuser vanes the maximum achievable efficiency is slightly lower due to the tip-gap losses but it can be reached over a broader range of flow.

An example that serves to illustrate the points above was a compressor system with four working point delineated in table 4.2. The difference in efficiency at each working point was evaluated.

It is important to note that having fixed diffuser vanes also limits the turndown and it is not possible to use the machine over a large range of flow coefficient; this is

why a variation of 30% of normalized flow coefficient is used in the example.

As expected at the two extreme required mass flow, the machine with fixed diffuser vanes is less efficient and suffers from high losses at the diffuser inlet. But over a narrow range it is actually more efficient than the configuration with adjustable diffuser vanes because there are no tip-gap losses in the diffuser.

Table 4.2: Specified performance test points and efficiency comparison of a system with adjustable diffuser vanes vs one with fixed diffuser vanes

Test points	Normalized Flow coefficient	Efficiency difference
1	50%	-8
2	65%	+2
3	70%	+1
4	80%	-5

4.6 Quasi-Steady Model

The Quasi-steady model builds on top of the system model and not only evaluates the optimal final values for the control parameters but also optimize the transition between the initial and the final state. In the water treatment industry the compressor speed has to be continuously adjusted to match the incoming varying flow of water that has to be treated.

4.6.1 Quasi-Steady Assumption

The compressor is assumed to work in a quasi-steady manner. The time presented here are non-dimensionalized using the rotor revolution time (time between 2 passages of the same blade), τ=t/t_{rotor}. The time it takes to move the vane actuators or change the impeller speed is compared to the time necessary to propagate a sound wave in the compressor and to the time it takes to convect any change of flow configuration. The convection time is defined as the meridional flow path over the meridional flow velocity. The meridional velocity of the flow varies with the flow coefficient so its
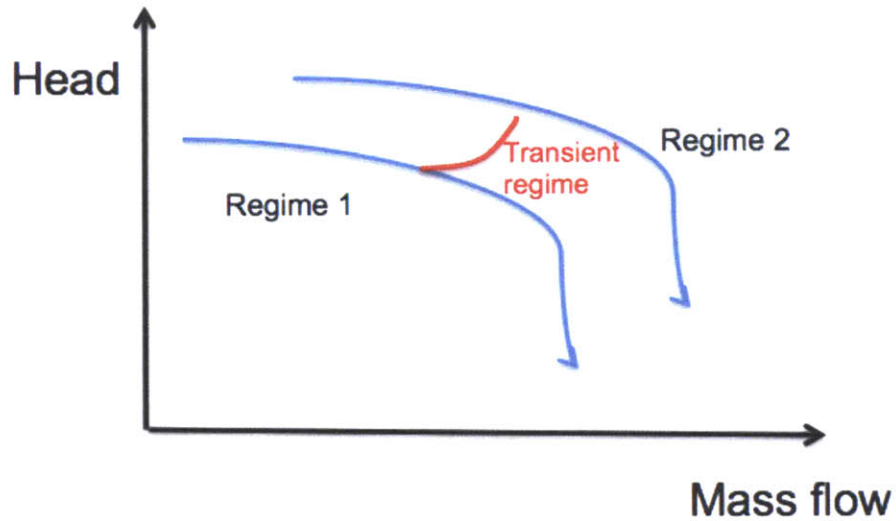
Figure 4-6: Transient regime

minimal value is used in order to calculate an upper bound characteristic time limit.

$\tau_{convection} = 250$

$\tau_{wave} = 25$

$\tau_{actuator} = 1250$

We have $\tau_{actuator} \gg \tau_{convection} \gg \tau_{wave}$ so the model can use the quasi-steady approximation.

4.6.2 Model Description

Another aspect of the control framework is its ability to optimize the transition between two working point. There are two main requirements, first, and by far the most critical, when going from one flow coefficient to another the compressor must not surge. A 20% safety margin was used to make sure this does not happen. Secondly, the energy used during the change must be minimized and the path with the highest efficiency has to be chosen.

The user selects the desired final flow coefficient and using the system optimization strategy presented above the algorithm determines the best final values for IGV and VDV angle setting and impeller speed. The model starts by changing the IGV until

60

it reaches the final IGV value. While doing so it also constantly adjust the impeller speed of the machine to stay away from surge. It then does the same thing with the VDV angle. When the VDV has reached its final angle the impeller speed is adjusted back to reach its optimum value.

For the current machine, the IGV has a large impact on the efficiency and on the turndown. for this reason, its change should be of first priority.

4.6.3   Quasi-Steady Model Results
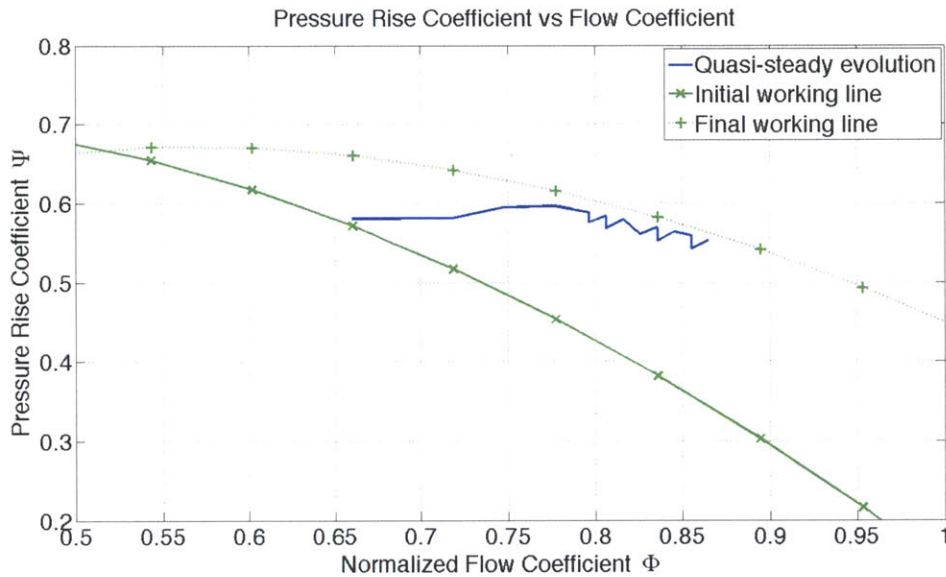
Figure 4-7: Calculated transient working point when changing operating conditions from a Normalized Flow coefficient of 0.65 to 0.87, with a fixed exit pressure

As an illustration, Figure 4-7 shows the computed behaviour of the compressor when increasing the flow coefficient. The models goes from IGV setting of 3,VDV setting of 4 and nominal impeller tip speed to reach IGV setting of 5, VDV setting of 4 and a 4.5% increase in the impeller tip speed. The exit pressure condition is assumed to stay constant so the impeller tip speed is adjusted in conjunction with the vane angle to reach the desired working point while having a constant exit pressure. The small irregularities in the curves are artefacts due to the discretization of the process and would not occur with a real machine. Thus the computed behavior of

the compressor operation based on the control framework can be tailored to meet the operating requirements.

4.7 Summary

This chapter presents the formulation of a the control framework that drives the compressor system for optimal performance characteristics. It is capable of continuously choosing the best value for the adjustable parameters (namely IGV and VDV angle settings and impeller speed) and minimizes the energy consumption at any flow coefficient.

The control framework can be adapted for centrifugal compressor system of different complexity; this includes configurations that have adjustable IGV and VDV angle, impeller speed or fixed nominal values for any of those parameters. In that case it evaluates what that fixed angle or RPM should be for a specific mission to maximize the average system efficiency.

Chapter 5

Computational Fluid Dynamics Assessment

5.1 Introduction

The meanline model has been assessed by comparing it to measured compressor map. Both the accuracy and the limitations of the model have been described earlier. The accuracy of the model was found to be good as long as the IGV setting angle stays small and if the region of interest is close to the working point with the highest efficiency. The model accuracy becomes limited as the operating point approaches choking.

Even when using the model in the range where it agrees with data, it is not possible to evaluate with a measured compressor map if the distributions of losses between all the components is correct. In order to measure the efficiency of the impeller it is necessary either to measure to total pressure right at the impeller exit (this will be discussed in the following chapter) or implement CFD simulations of the impeller.

This chapter describes how the CFD simulations of the impeller are carried out, and what phenomena and sources of losses can be analysed using CFD. The velocity field, the impeller slip and the tip-leakage flow are assessed.

5.2   Tools and Geometry
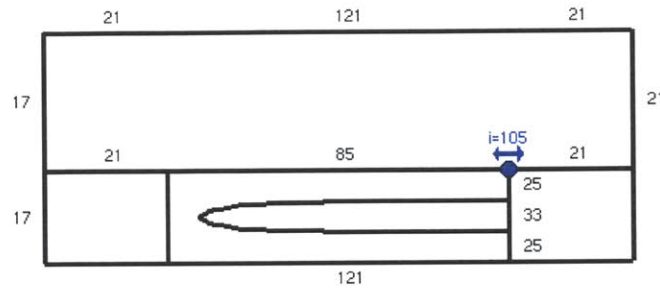
Figure 5-1: HI topology and details of the meshing process
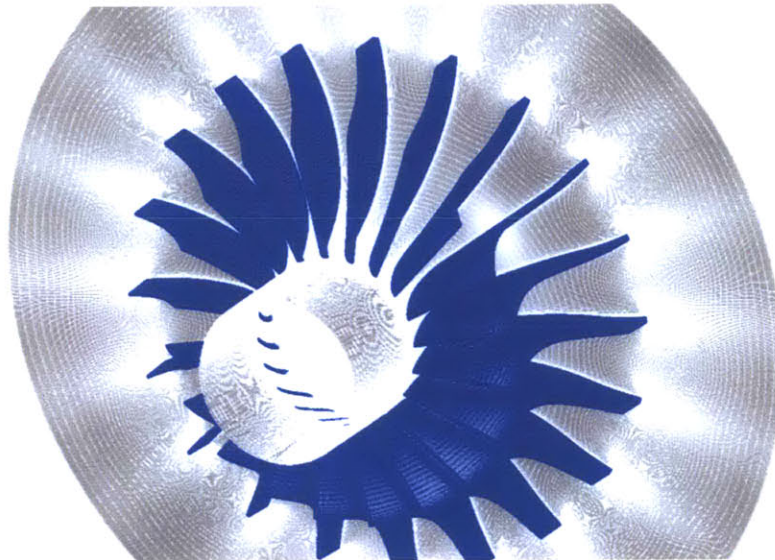
Figure 5-2: The generated impeller mesh for RANS computation

The impeller and its passage were meshed in Autogrid v5 and Numeca was used to calculate the flow. An analysis of the mesh was done and several meshes were compared. Several size and topology of meshes were tested and it was decided to use a 1 200 000 cells mesh with an HI topology as shown on Figure 5-1. This topology is especially adapted for centrifugal impellers with splitter blade (which is not the case here) but it was also the topology that produced the mesh with the highest quality. The meshed impeller can be shown in figure 5-2.

The diffuser was not meshed and a small converging flow section was added aft of the impeller in order to prevent backflow and allow the convergence of the simulation.

All the calculations were done using Reynold-Averaged Navier Stokes equations with Shear Stress Transport turbulence models. The difference in computed results with the use of Spalart-Allmaras model was not found to be significant in the situation here.

5.3 Assessing the Assumed Impeller Blade Surface Velocity Distribution

The impeller blade velocity distribution was assumed to be rectangular in the mean-line model and all the losses created by the impeller were evaluated based on that assumption. Its adequacy and its limits will be assessed using the computed results (from the use of CFD tool NUMECA).

5.3.1 Velocity Field in the Passage

Figure 5-3: Impeller Normalized velocity field at a Normalized Flow Coefficient of 0.53 and 50 degrees of pre-swirl

Figure 5-4: Impeller Normalized velocity field at a Normalized Flow Coefficient of 0.60

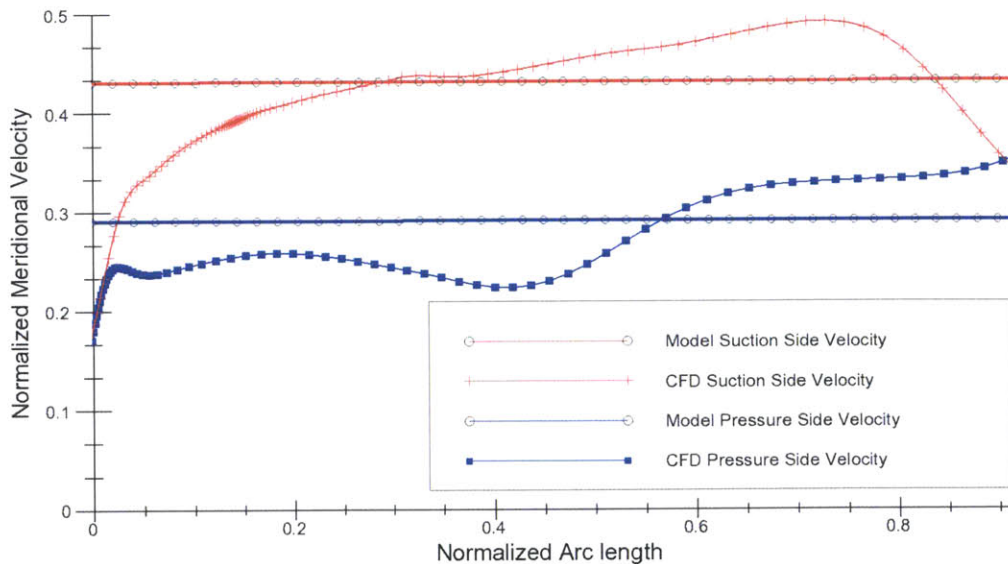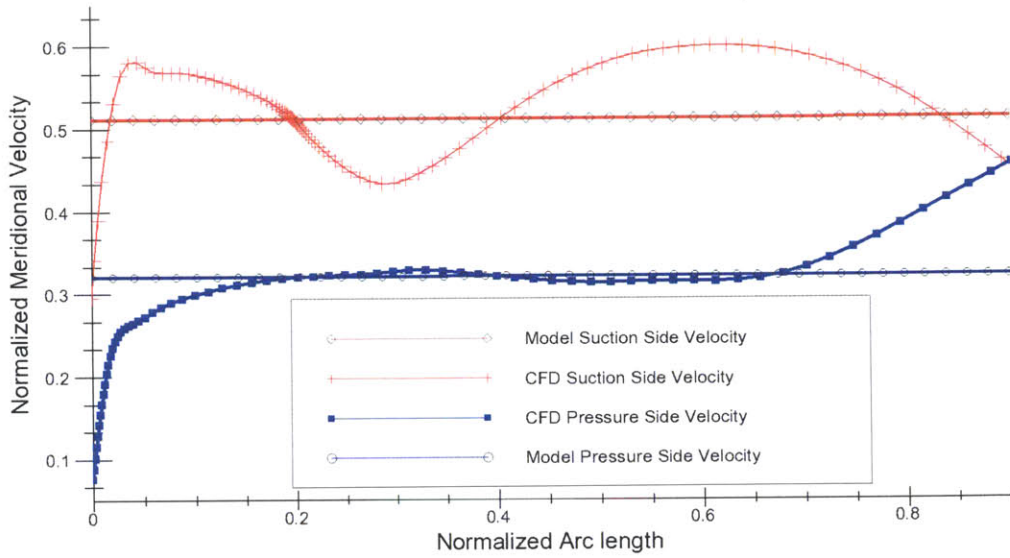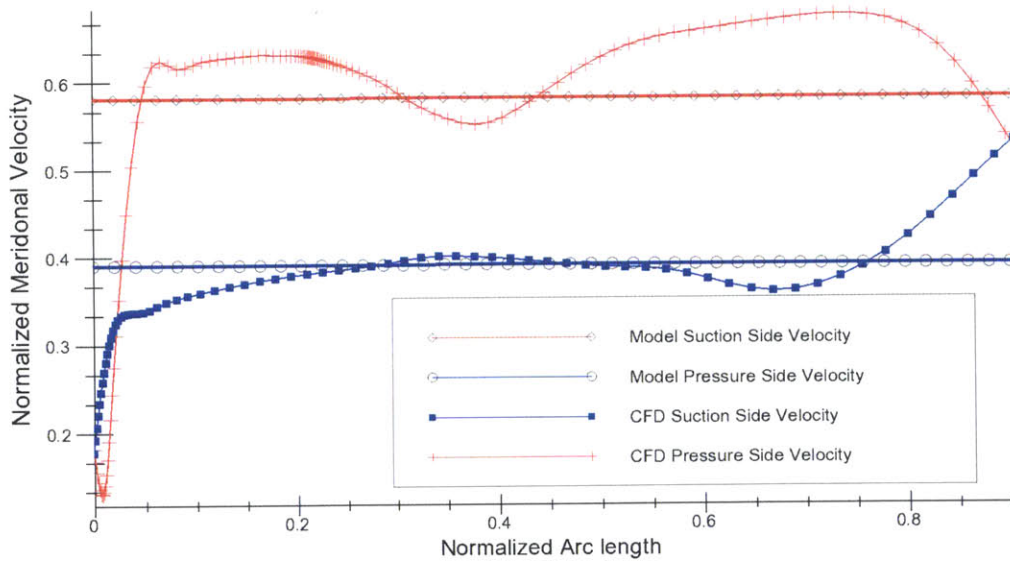Figure 5-5: Impeller Normalized velocity field at a Normalized Flow Coefficient of 0.72

The velocity in the impeller was mass-averaged from hub to shroud in all the simulations. The assumption of a rectangular velocity profile around the impeller was assessed by computing the averaged, from hub to shroud, velocity on both side of the impeller. The influence of the IGV angle and the flow coefficient was assessed as well.

It was found that under operating conditions of high efficiency with low vane angles the assumption made on the velocity field is valid. In the computed results shown in Figure 5-3 and Figure 5-4, for two different operating conditions, the pressure side of the impeller is well approximated (in terms of rectangular velocity distribution). The velocity on the suction side is within 20% of the computed velocity distribution.

When the flow coefficient is low with high pre-swirl from the IGV, the suction side of the impeller has an almost linear velocity profile and an improved approximation would be to use a triangular velocity profile distribution.

The rectangular velocity profile used works well in nominal working conditions. To estimate the error associated with using a rectangular velocity profile instead of using the computed velocity distribution from CFD the relative error incurred upon using the rectangular profile was estimated based on equation 5.1 and are presented in table 5.1. It is assumed that all the losses on the impeller blade scale as the cube of the meridional velocity Vm.

$$\Delta_{velpro} = \frac{\int_0^1 Vm_{model}^3 - Vm_{CFD}^3}{\int_0^1 Vm_{CFD}^3} \tag{5.1}$$

Table 5.1: Error in loss evaluation on the impeller for three different flow coefficient

Normalized Flow coefficient	0.72	0.60	0.53
Inlet Swirl in degrees	0	0	50
Pressure side losses relative Error in %	8.72	1.47	9.65
Suction side losses relative Error in %	3.24	3.17	6.38

While the velocity can vary by up to 20% from its expected value in one of the flow situation presented above, the error in loss estimation is less than 10% as seen in table 5.1. Approximating the impeller blade surface velocity distribution as rectangular for low pressure-ratio impeller is justified.

5.3.2 Impeller Exit Flow Angle Assessment

The exit flow angle relative to a reference angle was calculated on a plane at the exit of the impeller. There is substantial flow angle variation in the tip-gap area due to the tangential velocity defect, so the flow is leaving the impeller almost axially with little swirl added by the impeller (this is not visible on Figure 5-6, 5-7 and 5-8 as they have been averaged from hub to shroud). As shown if Figure 5-6, 5-7 and 5-8 the flow angle is different on the suction side and on the pressure side of the blade. The deviation being up to three times larger on the pressure side. The computed flow angle variation from the suction side to the pressure side is in agreement with the jet-wake model of Dean and Senoo [5].

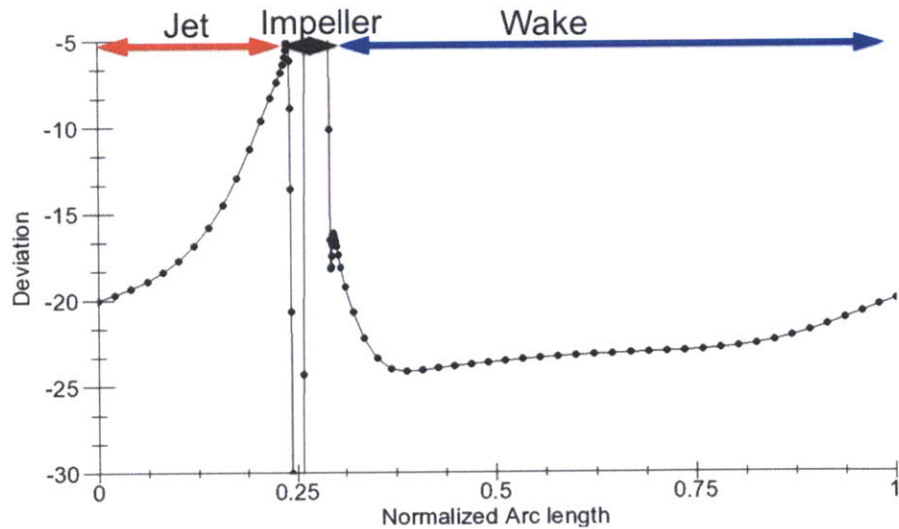Figure 5-6: Averaged Impeller exit flow angle in degree relative to a reference angle, normalized flow coefficient of 0.6
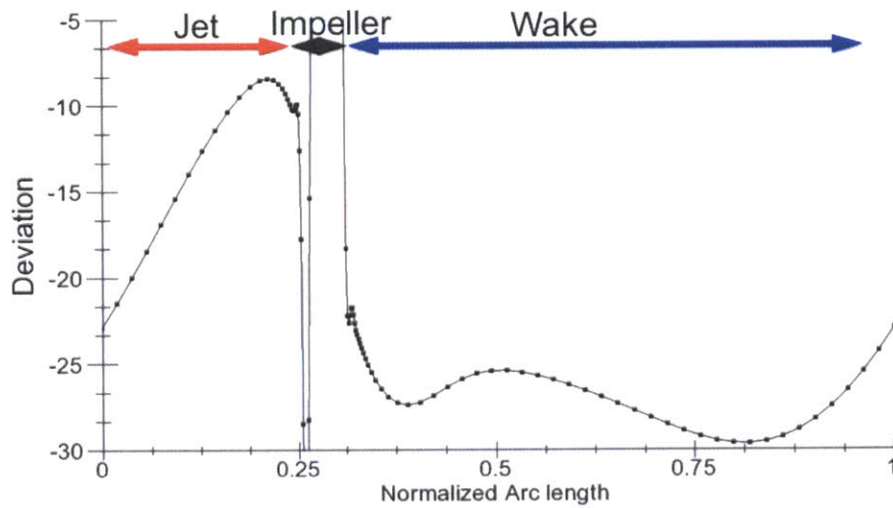
Figure 5-7: Averaged Impeller exit flow angle in degree relative to a reference angle, normalized flow coefficient of 0.72
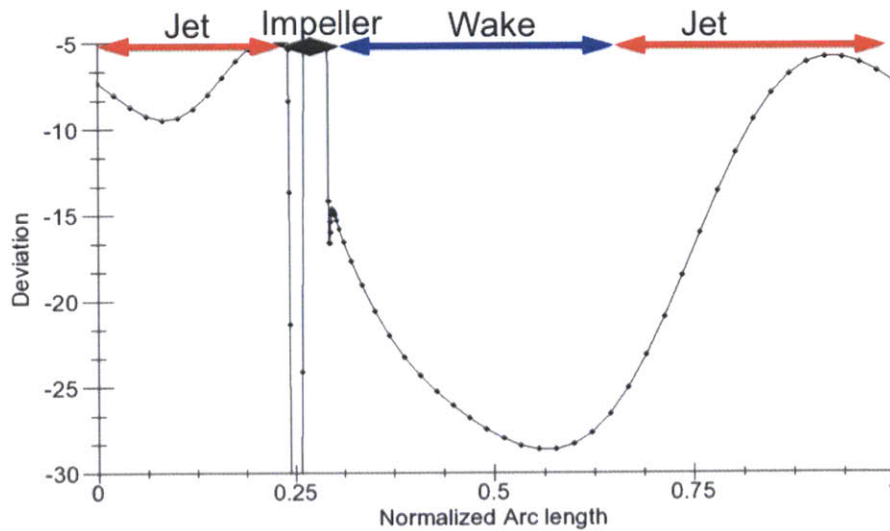

Figure 5-8: Averaged Impeller exit flow angle in degree relative to a reference angle, normalized flow coefficient of 0.72 with 50 degrees of pre-swirl

The relative error in the flow deviation angle was calculated by comparing the CFD averaged exit flow angle and the flow angle estimated from the mean-line model using the slip factor, these results are shown in table 5.3.

Table 5.2: Relative error in flow angle estimation using mean-line model against CFD computed results

Normalized Flow coefficient	72%	60%	53%
Inlet Swirl in degrees	0	0	50
Exit flow angle relative error	8.1	6.4	24.2

As expected, at high inlet swirl the results from the model do not match the CFD (or the experimental data) results. Since the impeller head rise is a function of the exit flow angle (from Euler Turbine equation), an incorrect estimate of the slip factor will lead to a large error in the calculated head rise. This implies that the model should be limited to low inlet swirl, i.e. low Inlet Guide Vane angle.

5.3.3 Loss Generation Associated with Impeller Tip-Gap Flow

An estimate of loss due to impeller tip flow is based on Denton's article [1]. As equation 5.2 below shows, it was necessary to evaluate the velocity on both the suction and the pressure side of the blade (which was done above) as well as the mass flow passing through the tip gap. Knowing the above quantities allows one to numerically evaluate the entropy generated by integrating equation 3.7 along the tip-gap. The compressor's tip-gap has a gap-to-height ratio of 3% if we take the inlet height as a reference but of 8% if we take the exit height as a reference. Figure 5-9 shows the clearance mass-flow distribution in the tip-gap from leading edge to trailing edge. The velocity in the tip gap normalized by the impeller tip speed is shown in Figure 5-10. Since the density in the compressor and the height of the tip-gap are constant, this plot is also representative of the mass flux distribution along the tip-gap. The leakage is maximum at the inlet of the impeller, where the loading is high so the difference in pressure between the suction and the pressure side of the impeller
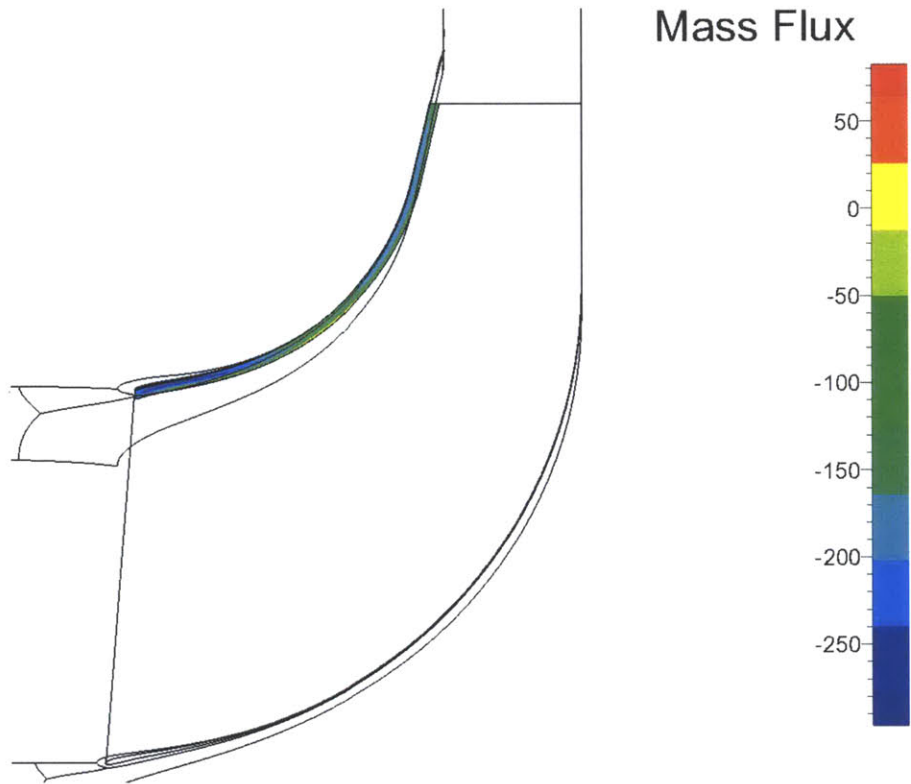
70

Figure 5-9: The mass flux distribution in the impeller tip-gap, negative sign indicates the flow goes from pressure to suction side
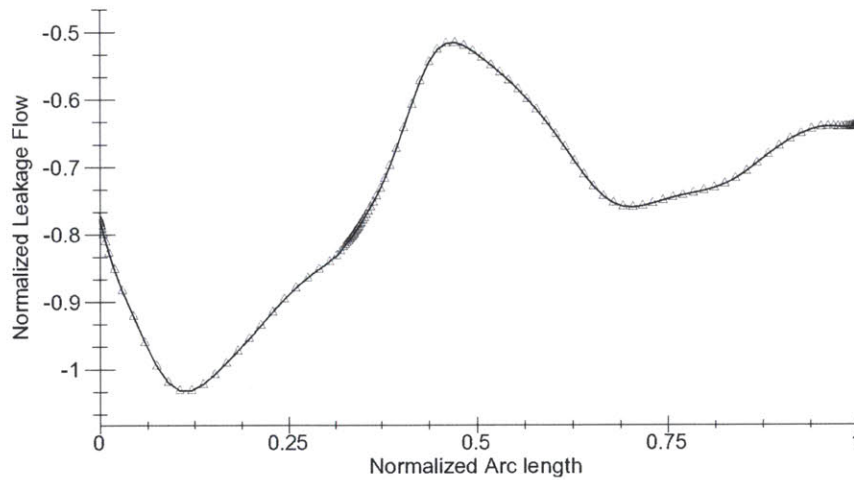

Figure 5-10: Normalized velocity field in the impeller tip-gap, negative sign indicates the flow goes from pressure to suction side

is also high. Using CFD allows us to precisely evaluate the losses without having to assume a rectangular velocity profile as what was done in the mean-line model.

The CFD calculations are compared to the mean-line model calculations using equation 5.2 in table 5.3.

$$\Delta \dot{m}_{tip-gap} = \frac{\dot{m}_{tg1D} - \dot{m}_{tgCFD}}{\dot{m}_{tgCFD}} \tag{5.2}$$

Table 5.3: Tip-Gap losses and mass flow comparison for three cases

Normalized Flow coefficient	72%	60%	53%
Inlet Swirl in degrees	0	0	50
% of mass flow through the tip-gap from CFD	10.6	9.6	9.5
Mass flow relative error meanline vs CFD in%	13.8	14.2	5.58

5.4 Stagnation Pressure Distribution at Impeller Exit

The distribution of stagnation pressure is computed on a plane at the exit of the impeller. The stagnation pressure is computed on a plane at the exit of the impeller to avoid including any losses in the vaneless space. The pressure coefficient is defined as $C_p = \frac{P_t - P_{atm}}{0.5 * \rho * U_2^2}$ and is shown in Figure 5-11. The hub-to-shroud distribution of stagnation pressure coefficient is computed using a circumferentially averaged flow field solution and is shown in Figure 5-12. It is inferred from the results of Figure 5-12 that the tip-leakage flow spans from shroud casing to 0.75 of the span. The computed results in Figure 5-12 is to be assessed against proposed experimental measurements.

5.4.1 Non Swirling Inlet Flow

Most of the computation done have a non-swirling inflow. The goal is to evaluate the stagnation pressure at the impeller exit, the exit flow angle, the effect of the tip- gap
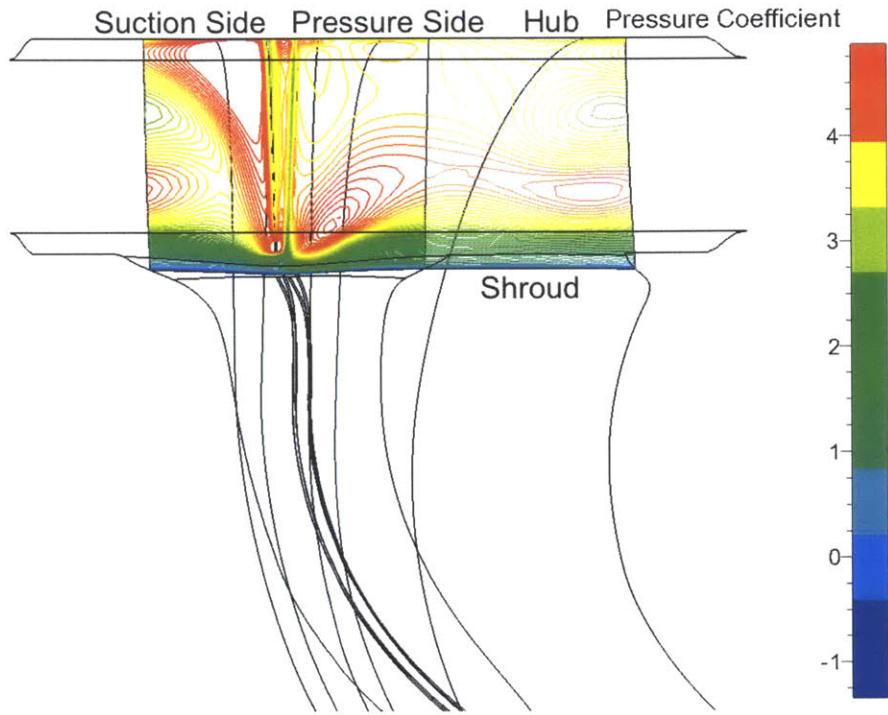
72

Figure 5-11: Pressure Coefficient field on a plane at the impeller outlet, the jet and wake are visible
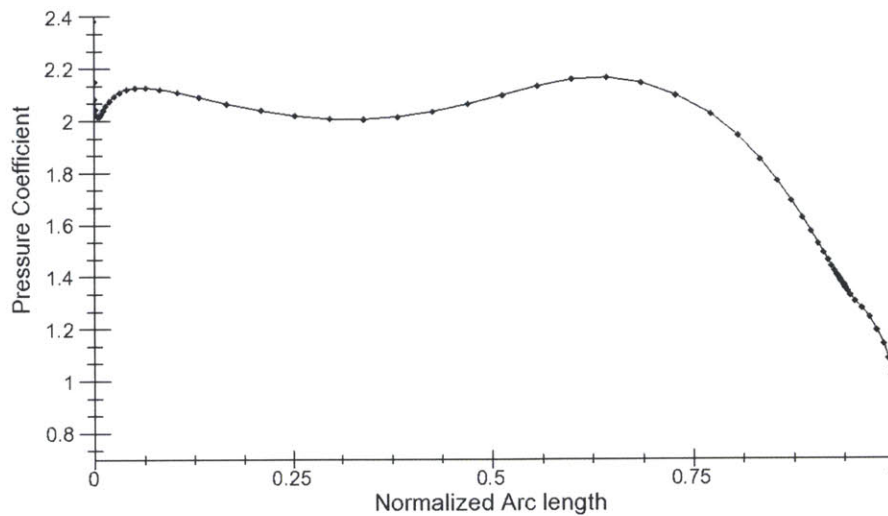

Figure 5-12: Pressure Coefficient distribution from hub to shroud at the impeller outlet. The low stagnation pressure flow due to the tip gap extends to about 25% of the passage

as well as an eventual boundary layer separation if it occurs.

With no swirl the IGV losses are negligible compare to impeller losses, the stagnation pressure at the impeller inlet is equal to the one at the IGV inlet. The stagnation pressure evaluated at the impeller exit will, under those conditions, give the impeller losses and efficiency. If this analysis is coupled with the experimental results, which provide the stagnation pressure at the compressor exit, the losses from the vaneless space, the diffuser and the volute can also be inferred. By knowing the stagnation pressure between the inlet and the outlet of a component its isentropic efficiency can be computed. The stagnation pressure at the impeller exit can both be computed and measured, and the stagnation pressure at the centrifugal compressor exit can be measured.

Since there is no measured or computed stagnation pressure after the diffuser it is not possible to decouple, in this case, the losses from the vaneless space, the diffuser, and the volute.

Table 5.4: Comparsion between the meanline model and the CFD impeller head rise

Normalized Flow coefficient	72%	60%
Inlet Swirl in degrees	0	0
Meanline Impeller Pressure Coefficient	1.91	1.95
CFD Pressure Coefficient	2.03	2.10
Relative error in %	5.9	3.3

The low relative error in table 5.4 indicates that for working point where no or little inlet swirl the model accurately evaluates the losses created by the impeller if the CFD is used as a reference.

5.4.2 Swirling Inlet Flow

The inlet boundary conditions of the solver were modified in order to simulate the effect introduced by a row of inlet guide vanes. Each impeller computation inlet flow

74

angle of 10, 30, 50 and 70 degrees were carried out. The tip-gap was set at its nominal value.

The goal here is to evaluate the impact of the IGV and to evaluate the pressure drop caused by their presence, especially at high angle. To do so both CFD and experimental results have to be used. The CFD will give the ideal pressure rise assuming the IGV do not add any loss and only impart swirl to the flow. Flow swirl angle is assumed to be equal to the IGV angle. While this assumptions holds at small to medium angles, for high IGV angles (30 degrees) there can be flow separation on the IGV blades. Using the CFD the impact of the IGV can be evaluated for different swirl angles and the results are displayed in Table 5.5 for three different IGV setting angle. Experimentally this can also be done as explained in Chapter 6.

Table 5.5: Impact of IGV swirl angle on impeller efficiency drop, large IGV setting adds little swirl

IGV setting	10	6	2
Impeller efficiency drop in %	2	5	18

5.5   Limitations

Some of the limitations are inherent to the type of CFD implemented: limited accuracy because of the grid resolution, steady calculations, Reynolds Averaged Navier Stokes equation approximation. Since the diffuser was not included it is assumed that no coupling occurs between the impeller and the diffuser. The Swirl created by the IGV is also assumed to be the IGV angle.

5.6   Summary

In this chapter rudimentary CFD RANS analysis of the impeller has been implemented. The diffuser has not been included but appropriate boundary conditions

reflecting the presence of the IGV was used. The losses caused by the tip-gap flow and the impeller slip were analysed. The stagnation pressure distribution was computed at the impeller exit. The computed results are also compared to those from the meanline model for assessing both qualitative and quantitative aspects. Overall, the results from the meanline model are in accord with those from the CFD computation. These results will be used in conjunction with the experimental measurements for inferring the IGV losses and the losses caused by the vaneless space, the diffuser and the volute.

Chapter 6

Experimental Setup for Measurements and Assessments

6.1 Methodology

To assess the accuracy of the 1D model and the loss distribution between the impeller and the diffuser, it is necessary to measure the total pressure at the exit of the compressor and in the compressor in between the different sections. Measured data at the exit of the compressor was already available and full compressors maps for various IGV and VDV angle were provided.

It was decided to modify the diffuser vanes to measure the total pressure and the flow angle right at the exit of the impeller. This measurement allows the decoupling of the losses occurring before and after the impeller. It allows one to evaluate the sum of the losses from the IGV and the impeller as well as the sum of the losses from the vaneless space, the diffuser and the volute. Since only the sum of the losses are known as illustrated in figure 6-1 and we want to evaluate the impeller losses, we need to evaluate the IGV losses. For low IGV angle setting, the total pressure drop across the IGV is negligibly small. The total pressure probe will then measure the total pressure rise from the impeller.

The difference between the total pressure at the exit of the machine and the one measured at the diffuser inlet is the pressure loss from the vaneless space, the diffuser and the volute.
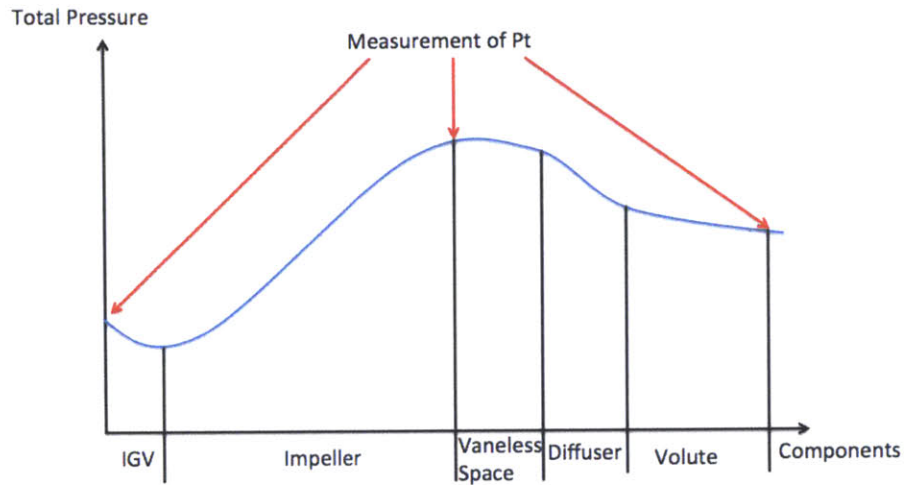

Figure 6-1: Evolution of the total pressure in the compressor

There is a need for more than one probe in order to measure a radial total pressure profile from hub to shroud; thus a set of diffuser vanes is incorporated with pressure probe to measure the total pressure at varying height in the diffuser passage.

Other diffuser vanes are modified to measure the flow angle. By using two probes placed at an angle with the flow, it is possible to measure the flow angle. Several vanes are modified in order to measure a broad range of flow angle. This value is then compared to the model and the slip factor can be evaluated.

6.2   Flow Angle Measurement

Diffuser vanes 6-3 were machined in order to measure the flow angle at the exit of the impeller, this allows one to evaluate the slip at the impeller exit and the swirl angle at various conditions. To do so, four pairs of blades were modified by adding pitot tube in them. Each pair of vanes has pressure sensors that are at $+30°$ and $-30°$ along a desired median angle as detailed in Table 6.1. The flow angle can be precisely measured if the flow makes the same angle between 2 probes; both probes
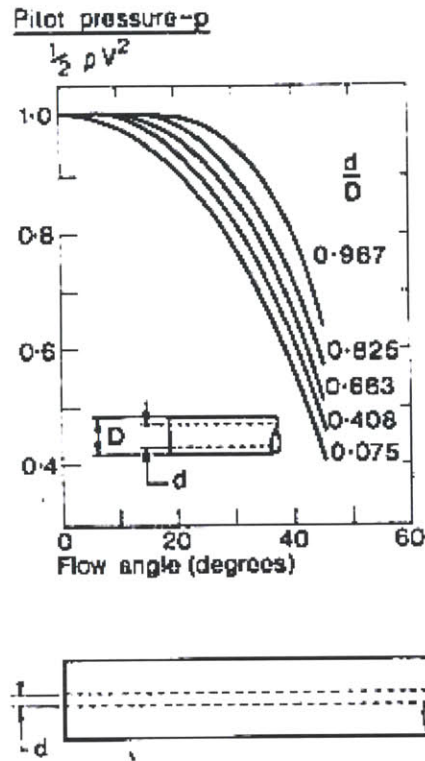
Figure 6-2: Reduced measured pressure vs flow angle, from Pankhurst [10]

Table 6.1: Angle of the axis of symmetry between 2 probes

| Median Angle between 2 probes | 5° | -2.5° | -7.5° | -10° | -15° | -20° |

will have the same pressure reading when the flow is at the median angle between the pair of pitot pressure sensor. Figure 6-2 was used to design the probe and estimate the pressure measurement as a function of the flow angle with the probe.

6.3   Total Pressure Measurement

Nine diffuser blades 6-5 were modified in order to measure the total pressure along the leading edge. Each vane has a pitot tube placed at various positions along the leading edge. This allows the measurement of a total pressure steady-state profile along the diffuser height. It is especially important to measure the total pressure next to the shroud to determine the deficit in stagnation pressure created by the
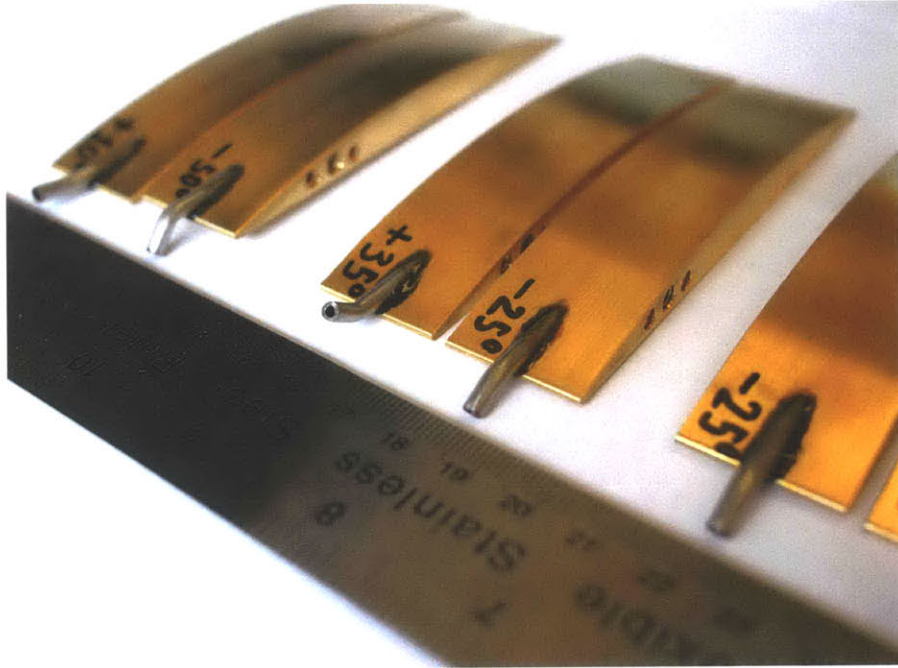
Figure 6-3: Close-up view of a pair of flow angle probes

Table 6.2: Position of Total pressure probes in % of the blade height

Position of vane in %	2.5%	12.5%	25%	37.5%	53%	69%	85%	98%

tip-gap as shown in Figure 6-4. The probe position is known using Table 6.2. The probes are designed to measure the total pressure from the hub to the shroud, and the probes are machined to be flat and face the flow as seen on Figure 6-5.

6.4 Uncertainties in Proposed Measurements

The positioning of the vanes and the probes is key. Since the flow angle will be a measured quantity the diffuser vane angle has to be known with a better accuracy than the expected resolution of the measurement. The measurements will be done with a low bandwidth sensors so an averaging of the pressure occurs and the high

80

Plane of measurement of the radial total pressure profile

Figure 6-4: Plane of measurement of the total pressure

frequency pressure variations are not measurable. For example the jet and wake component of the flow leaving the impeller cannot be measured.
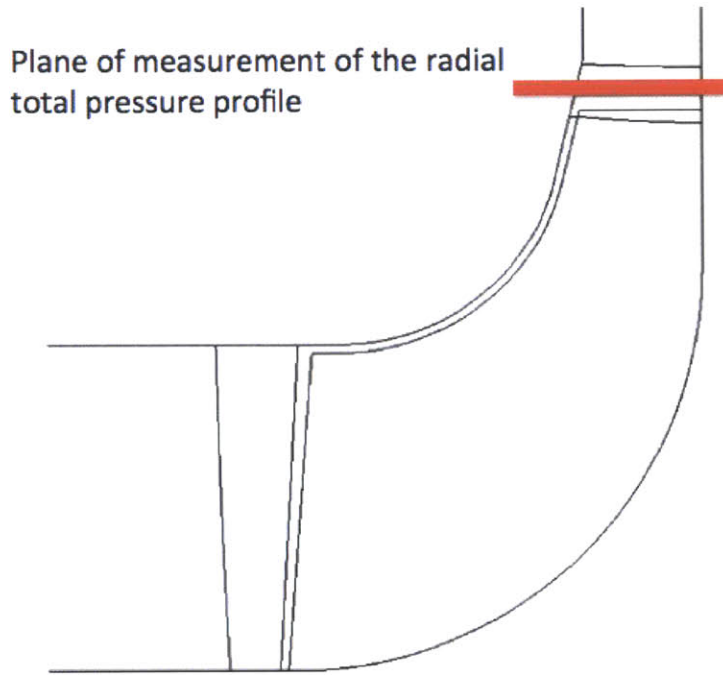
Since the probes are placed in the vicinity of the impeller trailing edge the pitot probes are subject to significant unsteady pressure field and the probes have to be designed to withstand the unsteady load that can occur. The resonance frequencies of the tube also have to be calculated in order to evaluate the precise pitot probe length that will prevent a resonance with the impeller blade passage passing frequency.

6.5 Control Framework Implementation

The control framework will be assessed by manually controlling the compressor. Since the control algorithm works in small steps and increments, it is possible to manually adjust the compressor to always follow the calculated working point. This is also the safer option as it allows the operator to quickly react in case of surge. For final and definitive implementation, the pre-calculated optimal position would be programmed

81
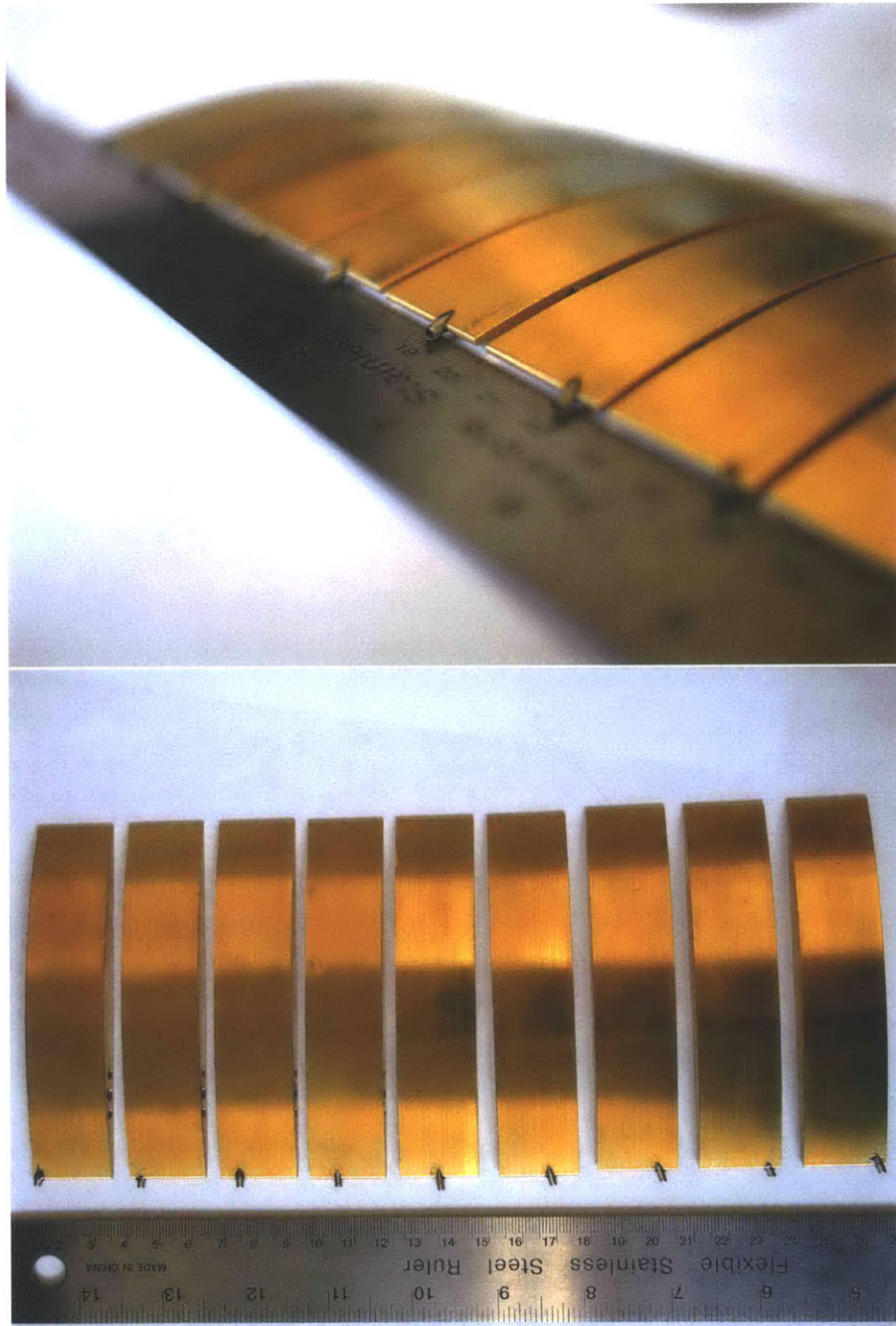
Figure 6-5: Total pressure probes on the diffuser vanes

in a module part of compressor rig control panel.

6.6 Summary

This chapter describes the proposed pressure measurement by fabricating probes on
the diffuser vanes leading edge. Two types of probes were manufactured, one to
measure the dynamic pressure and one to measure the flow angle relatively to the
diffuser blade. Both the losses created by the impeller and the slip angle of the flow at
the impeller exit are the main quantities of interest in this experimental protocol, the
resulting measurements will provide data for assessment against the meanline model
as well as the CFD computed results.

Chapter 7

Summary and Conclusion

7.1 Summary

This thesis assesses the characteristics of a centrifugal compressor system and the losses that occur in the system. Loss models are used to develop a meanline model of the compressor. This model is then used within a control framework that incorporates the effects on performance from varying IGV angle setting, impeller speed and VDV angle setting. The control framework is then implemented to demonstrate its utility in driving centrifugal compressor system to operate in a desirable manner to meet the requirements of a specific mission. Flow field computation using CFD and experimental measurements are proposed to assess the meanline model and identify the main losses. Impeller flow field computations were completed. Results from the meanline model are in accord with those from computation while instrumentation have been fabricated on the compressor test rig, the measurements of which are yet to be undertaken.

In terms of the research questions posed in Chapter 1, we have to a large extent (though not entirely) addressed the followings:

- The attributes of centrifugal compressor design and operation for achieving a broad operable performance characteristic with high efficiency retention.

- The parameters of high leverage that affect centrifugal compressor performance

on an effective basis to meet its mission requirements.

- An effective control strategy for achieving desirable compressor performance requirements for a specified mission at an optimal cost.

- The functional dependence of the non-dimensional performance parameters to improve the controllability and behaviour of the compressor on a beneficial basis.

- Definition of physical experiments for assessments of ideas and results

- Influences, limitations, and possible mitigation/control strategy for near matching of compressor components at all required operating points

As of to-date the main sources of losses on a centrifugal compressor have been assessed and a model for loss estimation has been developed except for the diffuser. The maximum achievable efficiency is evaluated (in the ideal limit of no losses) to compare with the provided experimental data. The effects of the IGV angle, the VDV angle and the flow coefficient have also been examined. The model provides a reasonable estimation of the IGV influence. The CFD analysis provides a baseline to compare the measurements to the computed flow. It allows the evaluation of specific losses such as the tip-gap losses. It also allows the assessment of the assumed impeller blade surface velocity distribution used in the meanline model since the velocity distribution of the flow on the suction and pressure side of the impeller can be calculated. The slip factor is also evaluated with the CFD and is in reasonnable agreement with the meanline model. The CFD analysis also allows qualitative analysis of the flow such as the visualization of the secondary flow or the location of separation of the flow.

7.2 Conclusion

We infer the followings based on implementing the model.

- The IGV provides a mean to reduce the compressor head with minimal efficiency drop for IGV angles lower than 20-30 degrees. Larger IGV angles lead to huge wake losses and are not recommended for achieving lower head; this is confirmed by the experimental data.

- The VDV has a significant impact on the operable range and there is a trade-off between efficiency and broad operating range; this is confirmed by the experimental data. The added complexity of adjustable diffuser vanes is justified only if the range of required mass flow is large enough. For compressor designed to work over a narrow range of massflows fixed diffuser vanes will give higher efficiency. The data also suggests that the optimal measured efficiency is close to the stall limit.

- The simple multi-parameter control strategy formulated could provide an operable and reliable framework for the compressor system to meet the requirements of a specific mission. It accommodates compressor configuration that have adjustable inlet and diffuser vanes or ones that have only adjustable inlet vanes. The limit of the control framework comes from the difficulty of the meanline model to precisely assess the onset of surge.

- Adjustable diffuser vanes improves the turndown by 40% while maintaining a constant efficiency. The VDV is used to maximize the efficiency at each working conditions.

- Adjustable IGV used at angle setting above threshold value result in substancial efficiency drop (large IGV angles are to be used only if it is critical to reach low flow coefficient with no concerns on the compressor efficiency penalty).

- The impeller tip-speed, which is adjusted by changing the drive motor RPM, is the most effective way to adjust the impeller head.

7.3 Recommendation for Future Work

The followings are recommended for future research:

I Acquire measurements in the compressor test rig to assess the meanline model for a representative range of IGV angle settings, VDV angle settings and impeller speed

II Implement the control framework on a representative centrifugal compressor system for assessments

III Improve meanline model and control framework using results from I and II above. This will include refining and improving loss models at high incidence angle and compressor surge criteria

IV Develop and implement a centrifugal compressor system design with full integration of the control framework to meet the requirements of an engineering mission.

V Quantify the benefits of a centrifugal compressor system where the control framework is integrated during the design and development phase compared to applying the control framework to an existing compressor system.

In addition, future research work should also be undertaken to complete the addressing of the many research question posed in Chapter 1. While the results presented in this thesis have addressed many aspects of the posed research questions, they have not been answered in their entirety on a quantitative basis.

Bibliography

[1] J.D. Denton *Loss Mechanisms in Turbomachines*,IGTI Scholar Lecture, 1993

[2] Marc Drela and Michael B. Giles and O'Dohrty T. *Viscous-Inviscid Analysis of Transonic and Low Reynolds Number Airfoils*,AIAA VOL.25 NO.10, 2001

[3] A.H. Shapiro. *The Dynamics and Thermodynamics of Compressible Fluid Flow*, Ronald, New York. 1953.

[4] T. Dickens , I. Day, *The Design of Highly loaded Axial Compressors*, Proceedings of ASME Turbo Expo 2009: Power for Land Sea and Air, 2009.

[5] N. A. Cumpsty, *Compressor Aerodynamics*, Krieger., 2004

[6] D.K.Hall,E.M. Greitzer, C.S.Tan *Performance Limits of Axial Compressor Stages*, ASME Turbo Expo, GT2012-69709, 2012.

[7] D.K.Hall,E.M. Greitzer, C.S.Tan *Performance Limits of Axial turbomachines Stages*, Master Thesis, 2011.

[8] J. Everitt, *The Role of impeller Outflow Conditions on the Performance and Stability of Airfoil Vaned Radial Diffusers*, Ph.D thesis, 2014

[9] E.M. Greitzer, C.S.Tan, M.B. Graf. *Internal Flows: Concepts and Applications*. Cambridge University Press, 2004.

[10] D.W. Bryer, R.C. Pankhurst. *Pressure-probe methods for determining wind speed and flow direction*. National Physical Laboratory, 1971.

[11] D. Japikse. *Radial Turbomachinery* ASME Turbomachinery Course, August 7- August 17, 1978.

[12] J. Helvoirt. *Centrifugal Compressor Surge Modeling And Identification for Control* Technische Universiteit Eindhoven, 2006

[13] H. Schlichting. *Boundary-Layer Theory*. McGraw-hill book company, 1979.

[14] J. Helvoirt, B. Jager, M. Steinbuch *Modeling and identification of centrifugal compressor dynamics with approximate realizations*. Proceedings of 2005 IEEE Conference on Control Applications, 2005

[15] W. Jansen *Improvements in Surge Margin for Centrifugal Compressors* AGARD, 1980